

Allan Amendola dos Santos

Recycled PS/TiO₂-Acetylacetone Nanocomposite as a Floating Photocatalyst

Dissertação de Mestrado

Dissertation presented to the Programa de Pós-Graduação em Engenharia Química, de Materiais e Processos Ambientais in partial fulfillment of the requirements for the degree of Mestre em Engenharia Química, de Materiais e Processos Ambientais

Advisor: Prof. Bojan Marinkovic



Allan Amendola dos Santos

Recycled PS/TiO₂-Acetylacetone Nanocomposite as a Floating Photocatalyst

Dissertation presented to the Programa de Pós-graduação em Engenharia Química, de Materiais e de Processos Ambientais of PUC-Rio in partial fulfillment of the requirements for the degree of Mestre em Engenharia de Química, de Materiais e de Processos Ambientais. Approved by the undersigned Examination Committee.

Prof. Bojan Marinkovic

Departamento de Engenharia Química e de Materiais - PUC-Rio

Prof. Anupama Ghosh

Departamento de Engenharia Química e de Materiais - PUC-Rio

Prof. Paula Mendes Jardim

Universidade Federal do Rio de Janeiro – UFRJ

Allan Amendola dos Santos

Graduated in Chemical Engineering by the Pontifical University of Rio de Janeiro – PUC-Rio in 2023. Areas of interest: Photocatalysis and Materials Engineering.

Bibliographic data

Santos, Allan Amendola dos

Recycled PS/TiO₂-Acetylacetone Nanocomposite as a floating photocatalyst / Allan Amendola dos Santos; advisor: Bojan Marinkovic. – 2025.

86 f.: il. color.; 30 cm

Dissertação (mestrado)-Pontifícia Universidade Católica do Rio de Janeiro, Departamento de Engenharia Química e de Materiais, 2025.

Inclui bibliografia

1. Engenharia Química e de Materiais – Teses. 2. Complexo de transferência de carga. 3. Reciclagem de poliestireno. 4. Remediação ambiental. 5. Nanomateriais suportados. 6. Fotocatalisadores flutuantes. I. Marinkovic, Bojan. II. Pontifícia Universidade Católica do Rio de Janeiro. Departamento de Engenharia Química e de Materiais. III. Título.

CDD: 620.11

Acknowledgments

I would like to express my deepest gratitude to my advisor, Prof. Bojan Marinkovic and Dr. Edisson Morgado for their guidance and support throughout the course of this research. Their expertise, insights and feedback were fundamental in the elaboration of this dissertation.

I would like to thank everyone on the research group of Centro de Pesquisa e Caracterização Avançada de Materais (CePeCAM), which I'm proudly part of, including Juliana, Lais, Marianne, Emanuel, Esteban and Gerson.

Finally, and most importantly, I would like to thank my friends and family. To my parents, Dennis and Mariane, for their unconditional love and belief in me.

This study was financed in part by the Coordenação de Aperfeiçoaento de Pessoal de Nível Superior - Brasil (CAPES) - Finance Code 001.

Abstract

Amendola dos Santos, Allan; Marinkovic, Bojan (Advisor). **Recycled PS/TiO₂-Acetylacetone Nanocomposite as a Floating Photocatalyst.** Rio de Janeiro, 2025. 86p. Dissertação de Mestrado — Departamento de Engenharia Química e de Materiais, Pontificia Universidade Católica do Rio de Janeiro.

Emerging contaminants are a new class of hazardous pollutants, mostly comprised of pesticides, fertilizers, dyes, and pharmaceuticals, commonly found in wastewater residues. Conventional wastewater treatment processes have often proven to be inefficient in the removal/degradation of these compounds. In this context, Advanced Oxidation Processes (AOPs), mainly Heterogenous Photocatalysis, have proven to be a promising alternative for pollutant degradation. Previous reports present TiO2-Acetylacetone Charge Transfer Complex (ACAC-CTC) as a viable photocatalyst for environmental remediation, as it promotes photodegradation reactions under visible light, while also retaining the innate advantages of titania. However, the use of powder photocatalysts imposes challenges in material recuperation and reusability, while also being prone to cause secondary pollution. Supporting photocatalyst powder at a polymeric matrix, such as polystyrene (PS), may be a viable solution to these drawbacks, especially if the composite exhibits floating capability. The present study aims to prepare and characterize PS/TiO₂-Acetylacetone nanocomposites through two different approaches, evaluate their photocatalytic activity in the photodegradation of tetracycline antibiotic under visible light irradiation and compare it to their powder counterparts. Thermogravimetric analysis proved both immobilization techniques to be efficient and composites specific surface area, calculated by BET method, were relatively high but significantly lower than the powder photocatalysts. While recuperation and reusability were potentially improved, photocatalytic activity of the nanocomposites suffered a severe reduction when compared to their powder photocatalyst counterpart, which was attributed to partial nanoparticle occlusion and poor reaction media coverage. Moreover, TOC results revealed that PS-based composites are prone to generating secondary pollution due to the release of microplastics and, possibly, PS photodegradation byproducts, which compromises their viability for environmental remediation purposes.

Keywords

Charge Transfer Complex; Recycled Polystyrene; Environmental Remediation; Supported Nanomaterials; Floating Photocatalysts.

Resumo

Amendola dos Santos, Allan; Marinkovic A., Bojan (Orientador). Nanocompósito de TiO2-Acetilacetona Suportado em Poliestireno Reciclado como Fotocatalisador Flutuante. Rio de Janeiro, 2025. 86p. Dissertação de Mestrado — Departamento de Engenharia Química e de Materiais, Pontifícia Universidade Católica do Rio de Janeiro.

Contaminantes emergentes são uma nova classe de poluentes, compostos principalmente por pesticidas, fertilizantes, corantes e produtos farmacêuticos, comumente encontrados em diversos efluentes. Os processos convencionais de tratamento de água e esgoto frequentemente se mostraram ineficientes na remoção/degradação desses compostos. Nesse contexto, os Processos Avançados de Oxidação (AOPs), principalmente a Fotocatálise Heterogênea, provaram ser uma alternativa promissora para a degradação destes poluentes. Estudos reportam o Complexo de Transferência de Carga (CTC) TiO2-Acetilacetona como um fotocatalisador viável para remediação ambiental, pois promove reações de fotodegradação sob luz visível, ao mesmo tempo em que retém as vantagens inatas da titânia. No entanto, o uso de fotocatalisadores sob forma de pós finos impõe desafios na recuperação e reutilização do material fotocatalítico, ao mesmo tempo em que é propenso a causar poluição secundária. Assim, a perspectiva de suportar fotocatalisadores em uma matriz polimérica, como poliestireno (PS), pode ser uma solução viável para essas desvantagens, especialmente se o material possibilitar sua flutuação. O presente estudo tem como objetivo preparar e caracterizar nanocompósitos de PS/TiO₂-Acetilacetona por meio de duas abordagens diferentes, avaliar sua atividade fotocatalítica na fotodegradação do antibiótico tetraciclina sob irradiação de luz visível e compará-la com o desempenho de fotocatalisadores em pó. Análises termogravimétricas provaram que ambas as técnicas de imobilização são eficientes e a área específica dos compósitos, calculadas pelo método BET, foram relativamente altas, mas significativamente menores do que as dos fotocatalisadores em pó. Enquanto a recuperação e a reutilização foram potencialmente melhoradas, a atividade fotocatalítica dos nanocompósitos sofreu redução severa quando comparada ao material não suportado, o que foi atribuído à oclusão de nanopartículas e ineficiente cobertura do meio reacional. Ademais, os resultados de TOC revelaram que os compósitos à base de PS são propensos a gerar poluição secundária devido à liberação de microplásticos e, possivelmente,

subprodutos da fotodegradação de PS, comprometendo sua viabilidade para remediação ambiental.

Palavras-chave

Complexo de Transferência de Carga; Reciclagem de Poliestireno; Remediação Ambiental; Nanomateriais Suportados, Fotocatalisadores Flutuantes

Table of Contents

1.	Introduction	15
2.	Literature Review	19
2.1	Principles of Heterogeneous Photocatalysis	19
2.1.1	Photocatalysis as an Environmental Remediation Technique	21
2.1.2	2 TiO ₂ -based Photocatalysts	25
2.1.3	B TiO ₂ Modification Strategies and Visible Light Sensitization	27
2.2 F	Floating Photocatalysts	30
3.	Objectives	40
3.1	General objectives	40
3.2	Specific objectives	40
4. Phot	Recycled Polystyrene-based TiO ₂ -Acetylacetone Floating tocatalysts for Antibiotics Degradation	41
4.1	Introduction	41
4.2	Materials and Methods	45
	1 Sol-Gel Synthesis of TiO ₂ -Acetylacetone Charge Transfer	44
4.2.2	2 Photocatalyst Immobilization onto Recycled Polystyrene Matrix	46
4.2.2	2.1 Non-solvent Induced Phase Separation (NIPS)	46
4.2.2	2.2 Thermally Induced Phase Separation (TIPS)	48
4.2.3	3 Characterization Techniques	49
4.2.4	4 Measurement of Photocatalytic Activity	52
4.3	Results and Discussion	53

4.3. ²	1 Characterization and Photocatalytic Performance of TiO ₂ -ACAC	53
	2 Characterization and Photocatalytic Performance of PS-based posites	62
	B Evaluation of Physical and Photochemical Stability of PS-based ting Photocatalysts	71
5.	Conclusions and Future works	74
6.	Appendix	76
7.	References	78

List of Figures

1s Atomic Orbitals (23)	20
Figure 2 – Effect of dimension on energy levels of MO's (23)	20
Figure 3 – Schematic representation of photodegradation process on the surface of a semiconductor (29)	22
Figure 4 – Band levels of various photocatalysts against standard hydrogen electrode redox potentials	23
Figure 5 – Schematic representation of charge carrier recombination process – Adapted (21)	24
Figure 6 – Representation of crystal structures of TiO ₂ polymorphs – Adapted (37)	26
Figure 7 – Schematic illustration of impurity energy levels of doped semiconductor (42)	28
Figure 8 – Charge transfer mechanism in three main types of heterojunctions (45)	29
Figure 9 – Visible-light sensitization mechanism of TiO ₂ through LMCT Complex	30
Figure 10 – PS/TiO ₂ -ACAC composite beads prepared by NIPS methodology	47
Figure 11 – PS/TiO ₂ -ACAC composite prepared by TIPS methodology	48
Figure 12 – XRD patterns of TiO ₂ -ACAC xerogel (a), TiO ₂ -ACAC270 (b) and TiO ₂ -ACAC300 and peak identification (d)	54
Figure 13 –N ₂ adsorption-desorption isotherms for TiO ₂ -ACAC CTCs	55
Figure 14 – TGA curves of TiO ₂ -ACAC CTC nanopowders	56
Figure 15 – FT-IR spectra of TiO ₂ -ACAC CTC nanopowders	57

Figure 16 – EPR spectra of TiO ₂ -ACAC CTC nanopowders	58
Figure 17 – SEM images of TiO_2 -ACAC300 nanopowders magnified by $1000x$ (a) and $5000x$ (b)	59
Figure 18 – TEM images of TiO ₂ -ACAC300 nanopowder	59
Figure 19 – Photocatalytic performance of TiO ₂ -ACAC CTCs for tetracycline degradation under visible light (24 W)	60
Figure 20 – UV-Vis spectra of tetracycline during photocatalytic tests with TiO ₂ -ACAC270 (a) and TiO ₂ -ACAC300, along with TOC presence in reaction media (c)	61
Figure 21 – TG curves of NIPS (a) and TIPS (b) composites/foams	62
Figure $22 - N2$ adsorption-desorption isotherms for NIPS (a) and TIPS (b) samples	63
Figure 23 – SEM images of pure PS-NIPS foam's surface (a, b) and PS-NIPS/TiO ₂ -ACAC300 (30%) composite's surface (c) and cross-section (d)	66
Figure 24 – SEM images of pure PS-TIPS foam's surface (a) and cross-section (b), along with PS-TIPS/TiO ₂ -ACAC300 (30%) composite's surface (c) and cross-section (d)	67
Figure 25 – Photolysis and photocatalytic performance of PS-NIPS/TiO ₂ -ACAC composites and pure TiO ₂ -ACAC300 under visible light (100 W) for TC degradation	68
Figure 26 – Photolysis and photocatalytic performance of PS-NIPS/P25 composites and pure P25 under UV light	69
Figure 27 – SEM images of PS-NIPS/TiO ₂ -ACAC300 (30%) surface (a, b) and interior (c, d) after photocatalytic tests	72
Figure 28 – TOC analysis of NIPS in the dark, under agitation (a) and under 100 W visible light irradiation and agitation (b)	72
Figure A1 – TG curves of PS-NIPS/P25 composites	76

76
77

List of Tables

Table 1 – Summary of the studies related to polymer-based floating photocatalyst for environmental remediation	34
Table 2 – Summary of the studies that applied PS-based floating photocatalysts for environmental remediation purposes	36
Table 3 – Reported specific surface areas of polymer-based floating photocatalysts	38
Table 4 – BET specific area of TiO ₂ -ACAC nanopowders	55
Table 5 – Experimental (BET) and theoretical specific areas of NIPS and TIPS samples	64
Table 6 – Density measurements of NIPs and TIPS composites	65
Table A1 – BET specific area of TiO ₂ -P25 and PS-NIPS/P25 composites	77

1 Introduction

Over the past century, accelerated urbanization and industrialization processes took place around the world, drastically changing the relationship between humans and the environment. Humanity quickly developed an increased dependence on fossil fuels for energy, as the continued growth of urban and industrial areas demanded more and more resources. Due to continuous unsustainable practices, numerous environmental problems have emerged, with the pollution of aquatic environments being among them. An alarming quantity of toxic and/or environmentally hazardous residues, originating from residences, factories, and agricultural activities, are inappropriately released in aquatic media to this day, which pose an immediate threat to various ecosystems and, possibly, to human health [1,2]. A new class of pollutants, known as emergent contaminants, which are commonly found in wastewater residues mostly comprised of pesticides, fertilizers, dyes and pharmaceuticals, have been the subject of various studies due to their potential toxicity and chemical stability, making them susceptible to bioaccumulation and biomagnification processes [3,4]. Emergent pollutants are also known for being particularly hard to degrade through conventional wastewater treatment processes [5]. Therefore, new sustainable techniques for the removal of these contaminants must be developed before more severe environmental impacts become a reality.

Among pharmaceuticals, antibiotics such as tetracycline have been frequently detected in natural water bodies due to their widespread use and low biodegradability. Tetracycline, in particular, is a broad-spectrum antibiotic that poses ecological risks even at low concentrations, contributing to the emergence of antibiotic-resistant bacteria. Therefore, developing efficient photocatalytic systems capable of degrading tetracycline under visible light has become a significant research goal [6,7].

To remove or degrade organic emergent contaminants from aqueous media, different technologies have been developed, such as the use of adsorbent materials, nanofiltration membranes, precipitation and coagulation [8,9,10]. Among these methods, the Advanced Oxidation Processes (AOP's) have been of particular interest in numerous studies due to their capability of degradation of various types of organic pollutants, often to the point of complete mineralization [11,12]. The degradation of organic compounds by AOP's occurs by the production of reactive oxygen species (ROS), such as 'OH (hydroxyl radical) and 'O2⁻ (superoxide radical), which then proceed to react with a pollutant molecule and convert it into the simpler and desirably non-toxic compound. In this context, heterogeneous photocatalysis is one of the most prominent and frequent subjects of studies among AOP's, due to its relatively low cost, high efficiency, sustainability, and simple application [11,12,13].

A wide range of semiconductors, generally in the form of transition metal oxides/sulfides, can be used as photocatalysts for degradation of organic species in aqueous media, such as ZnO, ZnS, WO₃, CdS, SnO₂ and especially titania, TiO₂ [14]. Titania-based photocatalysts are commonly applied for this purpose, due to their high chemical stability, non-toxicity, biocompatibility and relatively low cost. However, due to its large bandgap of approximately 3.2 eV, TiO₂-based photocatalysts present very low absorption of visible light and, in addition, high electron-hole recombination rates, which hinder the effectiveness and applicability of the material as a visible light photocatalyst [15,16]. To overcome these drawbacks, among many different approaches, surface modification may be performed to the neat TiO₂, by coupling organic bidentate molecules such as acetylacetone (ACAC), to form a charge transfer complex (CTC) which is sensible to visible light and less prone to electron-hole recombination [1,16].

TiO₂ photocatalysts, as well as other semiconductors, are often used in the form of nanometric powders for pollutant abatement in the aqueous medium, to maximize surface area and, consequently, enhance photocatalytic performance [17]. However, powdered materials have inherent disadvantages such as expensive and difficult recoverability, high mobility of fine powders which can be hazardous to human health, and in some cases, low absorption of visible light in water bodies

deeper than 0.5 m [15]. Therefore, immobilization of TiO₂ particles onto a suitable floating support is an interesting alternative to overcome those drawbacks [18,19].

To be used as such a support, the material must meet certain requirements, such as high affinity (adhesion) to the active phase, high chemical stability specially to oxidizing free radicals, grant high specific area, and low density, if floatation is desired. Different types of materials, with various morphologies, may be used as supports for photocatalysts [15]. Polymeric foams appear to be rather promising in this regard; the possible formation of tridimensional porous networks grant a high specific area and low specific mass, while also being possible to prepare from recycled polymeric waste [18]. A fair number of polymers may be used as support material; however, expanded polystyrene (PS), commercially known as StyrofoamTM, is an excellent option since it is broadly available, inexpensive, and has unexplored recycling potential [20].

Although heterogeneous photocatalysis as an environmental remediation technique has been widely investigated in the literature, the use of PS as a support for photocatalytic nanoparticles would repurpose said polymeric waste, which, as highlighted by de Souza Cunha *et al.*, has difficult recyclability [20]. Also, as far as the authors know, there are no reports on the use of TiO₂-Acetylacetone (TiO₂-ACAC) charge transfer complex supported on any kind of substrate, for photocatalytic purposes, which in turn, could improve recoverability and multiple cycle usage of a photocatalyst that's both efficient and sensitive to visible light. Considering this, the present work's objective is to prepare and characterize a photocatalytic composite, by applying polystyrene waste as a floating support for TiO₂-Acetylacetone charge transfer complex used for antibiotic photodegradation under visible light, while also investigating the photochemical stability of the polymeric matrix.

This dissertation is divided into five chapters, including this introduction, as follows:

- Chapter 2: Literature Review on heterogenous photocatalysis, visible light sensitization strategies for TiO₂ photocatalysts and floatable supports for photocatalysts
 - Chapter 3: Objectives

- Chapter 4: Polystyrene-based TiO₂-ACAC Floating Photocatalysts for Environmental Remediation (Manuscript)
 - Chapter 5: Conclusions and proposals for future works

2 Literature Review

2.1 Principles of Heterogenous Photocatalysis

Photocatalysis is a broad term, which, according to IUPAC, is attributed to change in rate of a chemical reaction and/or reduction of its activation energy under irradiation of light, in the presence of a photocatalyst [21]. It also may be classified as homogenous, when the photocatalyst and reactants coexist in the same phase or, more commonly, as heterogenous, when the photocatalyst and reactants present themselves in different phases [22]. Photocatalytic materials may be used to lower the energy activation of non-spontaneous chemical reactions ($\Delta G > 0$), enabling photosynthetic processes where photon is considered to be an active reactant, such as in water splitting and CO₂ reduction. Alternatively, photocatalysts may be used to enhance the kinetics of already spontaneous reactions ($\Delta G < 0$), by altering its reaction routes, through absorption of photons, in processes such as oxidation of organic compounds [23].

Homogenous photocatalysts have really niche applications, when compared to their heterogeneous counterpart, for numerous reasons, but mainly due to their high solubility in the reaction media, which makes its separation and reusability notoriously difficult [24]. Furthermore, heterogenous photocatalysts are usually simpler to synthesize and can be modified to absorb visible light and enhance photocatalytic activity, hence are more commonly found in literature for several photocatalytic processes. Ceramic semiconductors are by far the most well-known type of heterogeneous photocatalysts, which include materials such as ZnO, CdS, SnO₂, WO₃, GaP and, especially, TiO₂ [14].

The photocatalytic properties presented by some semiconductor materials can be understood by the Molecular Orbital Theory. Chemical bonding occurs when two adjacent atoms, at an optimal distance from each other, have their own individual atomic orbitals (AOs) overlap to form molecular orbitals (MO). Due to the wave-particle duality of electrons, the interaction of wavefunctions of each

contributing AO can be either constructive, resulting in a bonding orbital MO, or forming an antibonding orbital MO. Formation of MO's can be pictorially represented as shown by Figure 1, where two 1s AOs are combined to form the two MOs [25], one bonding and another one, antibonding.

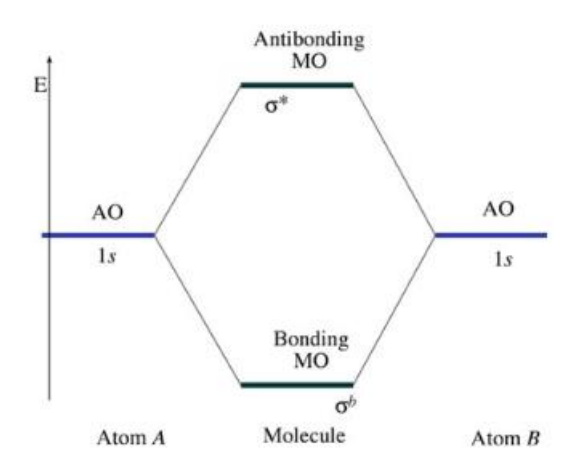


Figure 1: Formation of Bonding and Anti-bonding MO's, starting from 1s Atomic Orbitals [25]

As shown in Figure 1, the combination of AOs of two adjacent atoms lead to the formation of bonding and antibonding MOs, each with their own quantized energy levels. However, when numerous atoms are brought together to form a solid material, the Pauli exclusion principle dictates that electrons cannot have the same set of quantum numbers, and, consequently, energy levels that were once identical in isolated atoms, shifting them relative to one another in a solid. Since a solid contains an enormous quantity of atoms, the MOs formed during bonding are so closely spaced in energy that they can be considered as continuous bands of energy levels. Figure 2 illustrates the effect of change in dimension on the energy levels of MOs [25].

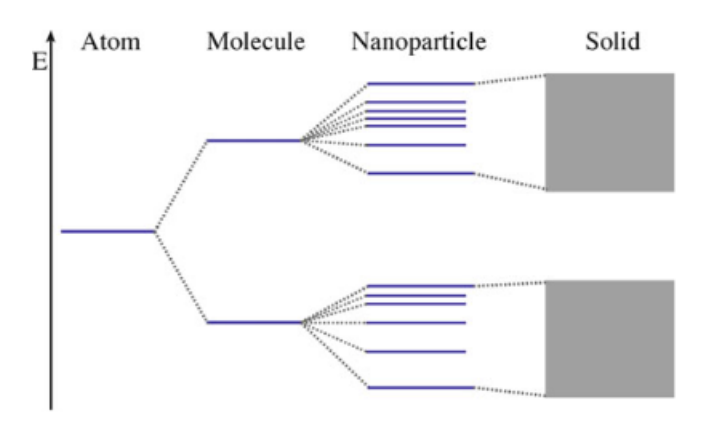


Figure 2: Effect of dimension on energy levels of MO's [23]

The overlapping energy levels of bonding MOs gives rise to the Valence Band (VB), whereas overlapping antibonding MOs generates the Conduction Band (CB). In their ground state, the VB is composed of bonding or non-bonding electrons in the outermost layer of the atoms, while the CB remains unoccupied. In the case of insulators and semiconductors, the VB and CB are separated by an energy barrier, called bandgap (Eg), which is, by definition, the necessary energy to excite an electron from the top of VB to the bottom of CB. It is important to note that, in the absence of a significant quantity of certain point defects, the bandgap of a pure semiconductor is an energy interval with no intermediate energy levels, therefore cannot be occupied by electrons [25].

The bandgap is of extreme importance for semiconductors, regardless of their applications, as it dictates the amount of energy needed to promote electronic transitions in the material. If the material is provided with energy equal or higher than the bandgap, whether it is of thermal, electric or radiant nature, an electron from the VB is promoted to the CB, becoming a free electron (e⁻) and leaving a positively charged hole (h⁺) in the VB [17,26,27]. The generated e⁻/h⁺ pairs are the core of the semiconductor functionality, whether in photovoltaic cells for energy generation, in electronic circuitry or, in the case of the present study, for photocatalysis [28,29].

In the context of heterogeneous photocatalysis, the control of the bandgap, the charge carrier recombination rate and the absorption capacity in the visible spectrum are determinants for the performance of semiconductors. These characteristics will be addressed in the following sections in relation to modified TiO₂.

2.1.1 Photocatalysis as an Environmental Remediation Technique

In the context of pollutant removal and/or abatement in aqueous or gaseous media through heterogenous photocatalysis, the photodegradation process is based upon a series of consecutive oxidation reactions that occur on the surface of the semiconductor, which can be summarized as follows: (i) adsorption of target molecule and water/solvent onto photocatalyst surface, (ii) absorption of photon

with an energy equal or higher than the semiconductor's band-gap, leading to the formation of a hole (h⁺) and a free electron (e⁻) in the valence and conduction bands, respectively, (iii) migration of the e⁻/h⁺ pair to the surface of the semiconductor, (iv) oxidation and reduction of water and oxygen adsorbed on the surface, by h⁺ in the VB and e⁻ in the CB, respectively, leading to the formation of hydroxyl radicals ('OH) and superoxide radicals ('O₂-), the so called Reactive Oxygen Species (ROS); (v) adsorbed target molecules react with radical oxidizing species, resulting in their degradation and formation of structurally simpler molecules, (vi) desorption of the degraded molecules and adsorption of new ones [30]. Figure 3 summarizes the photodegradation process of organic pollutants on the surface of a photocatalyst. Given the previous step by step explanation of photodegradative process on semiconductors, key factors that influence the photocatalytic activity must be introduced and clarified.

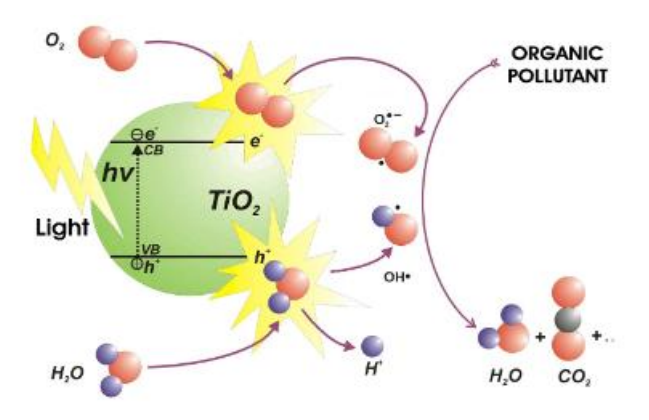


Figure 3: Schematic representation of photodegradation process on the surface of a semiconductor [31]

First and foremost, the band-gap energy and VB and CB energy levels play a vital role in photocatalytic activity, as well as the redox potential of the adsorbate. On the surface of the semiconductor, excited electrons in the CB might be donated to reduce an electrophilic species, while holes in the BV might accept electrons from a nucleophilic species, oxidizing it. However, the probability and rate of these events depend on the position of both the BV and CB relative to the redox potential of the absorbate. Reduction only occurs if the reduction potential of the electron acceptor is below the CB potential of the semiconductor, whereas oxidation only occurs if the oxidation potential of the electron donor is above (less positive than) the BV potential of the semiconductor [17]. Consequently, it can be inferred that

not all semiconductor photocatalysts are able to produce both hydroxyl and superoxide radicals, and therefore, may not be able to degrade certain organic compounds, as some have higher affinity with a certain ROS [30]. Figure 4 shows the band-edge positions of different photocatalysts, in relation to a standard hydrogen electrode.

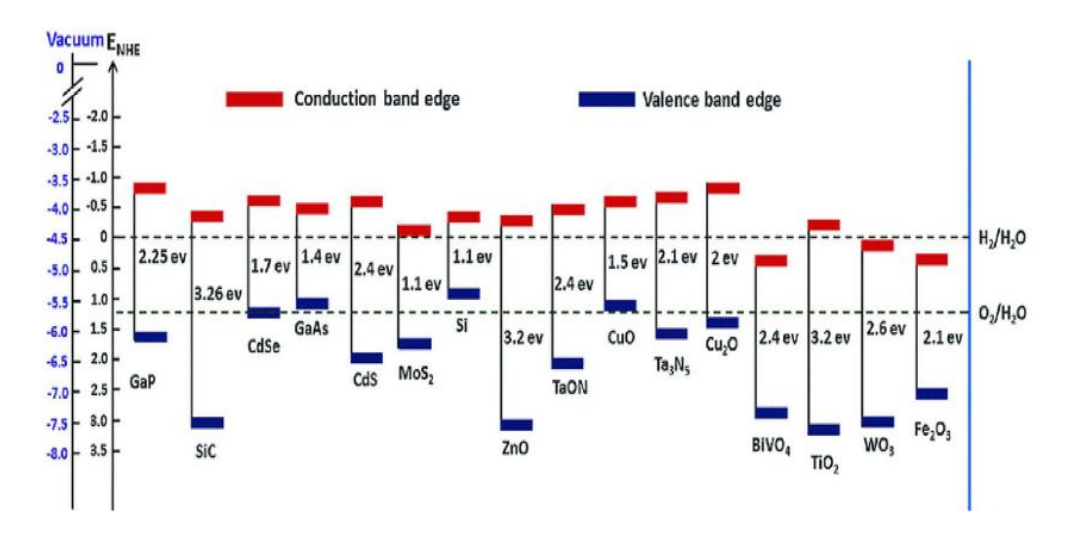


Figure 4: Band levels of various photocatalysts against standard hydrogen electrode redox potentials [28].

The bandgap energy corresponds to the photon energy that needs to be absorbed to promote electron excitation from the BV to the CB. Semiconductor materials may be capable of absorbing light in the IR, visible or UV spectrum, which, theoretically, dictates what sources of light are applicable to a certain photocatalyst [17]. For instance, Cu₂O bandgap energy ranges within 2.0-2.5 eV, which corresponds to wavelengths in the visible spectrum, whereas TiO₂ bandgap of 3.2 eV, mostly absorbs light in the UV spectrum [32] [33]. It should be mentioned that photocatalysts can undergo surface and bulk modifications to promote sensitization to visible light, as will be discussed in more detail in Section 2.1.3.

Another key factor that severely hinders photocatalytic activity is the recombination of charge carriers, as illustrated in Figure 5. Upon excitation, the e⁻/h⁺ pairs on the semiconductor surface can participate in redox reactions, as previously discussed (or recombine in bulk of the photocatalyst) in a process that competes with the formation of ROS. Typically, photocatalysts with low bandgap energy, require less energy for photoexcitation when compared to one with high bandgap energy, however they are also more susceptible to higher e-/h+

recombination rates [34]. As was the case of light sensitization, photocatalysts may also be engineered or modified to decrease charge carrier recombination rates.

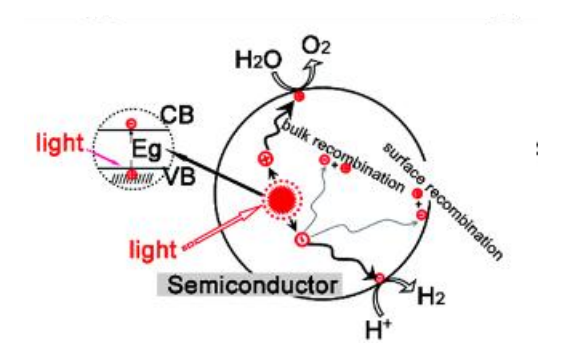


Figure 5: Schematic representation of charge carrier recombination process - Adapted [23]

From the factors cited so far, it can be concluded that not all semiconductors may act as photocatalysts. If bandgap energy is too high, visible light absorption is likely minimal or non-existent, which severely limits the applications of the photocatalyst for pollutant degradation. Conversely, if the bandgap energy is too low, not only is the semiconductor more susceptible to charge carrier recombination, but also it may not be able to produce the oxidizing radicals required for photodegradation reactions [30,34]. Chemical stability of the semiconductor is also paramount to its effectiveness as a photocatalyst, since it will be in direct contact with highly reactive oxidizing species. For instance, even though ZnO has a bandgap energy comparable to TiO₂, it is prone to photocorrosion under bandgap excitation [35].

Photocatalysts dimension also play an important role in photocatalytic performance; photocatalytic nanoparticles are especially relevant due to a few factors. Firstly, nanoparticles present a high surface area, usually in the order of 10² m².g⁻¹, which not only ensures a broader coverage of the reaction medium but also provide additional active sites, at which target molecules can be adsorbed. Additionally, due to the small diameter of nanoparticles, transfer of e⁻/h⁺ pairs from the bulk to the surface of the semiconductor is more efficient, usually resulting in higher redox reaction rates. Lastly, if nanoparticle diameter is less than a critical limit, usually comparable to the de Broglie wavelength of charge carriers of the semiconductor, quantum size effects start being relevant, as generated electrons and holes are not subjected to delocalization as in a bulk material. Quantum

confinement promotes discretization of electronic states inside the BV and CB and increases effective band gap energy. As a result, not only changes of material color can be observed but also different oxidation reaction rates [17,28].

Aside from the intrinsic properties of the photocatalyst, such as band-gap energy and particle size, certain external factors can severely affect the photocatalytic process. First and foremost, chemical composition of the reaction media must be known prior to any photocatalytic tests, as certain species may act as ROS scavengers and hinder the degradation of a target compound. For instance, anions such as Cl⁻, HCO₃⁻ and NO₃⁻ are notorious OH scavengers [36]. Photocatalyst concentration directly impacts photodegradation kinetics, as higher photocatalyst amount promotes formation of more oxidizing radicals. However, an excess of photocatalyst loading may induce light scattering and reduction of light penetration, possibly compromising reaction kinetics. Light power is also an important parameter in photocatalytic processes, as higher power leads to greater conversion rates of pollutants due to higher number of photons taking part in process. In addition, temperature of reaction media plays a key role in photocatalytic activity, as higher temperatures usually lead to greater rates of charge carrier recombination and pollutant desorption from photocatalyst surface, significantly impacting photodegradation kinetics. The presence of inorganic ions or organic matter may also affect the photodegradation process, as they may occupy photocatalyst's active sites and react with ROS instead of the target pollutant. Also, pH can alter photocatalyst surface charge, which in turn can either increase or decrease its affinity with the target compound. Additionally, the change in surface charge may also influence the size of agglomerates formed, reducing photocatalyst coverage of the reaction media [28,37].

2.1.2 TiO₂-based Photocatalysts

Regarding semiconductor materials with photocatalytic properties, TiO₂ plays a vital role, being the most used photocatalyst. The relevance of TiO₂-based photocatalysts is due to its many advantages such as chemical stability, non-toxicity, low cost and broad availability. Furthermore, regarding photocatalysis as an AOP for environmental remediation, TiO₂ is especially relevant, since the

positioning of the valence and conduction bands relative to the redox potential of water and oxygen, enables TiO₂-based photocatalysts to produce both 'OH and O₂-radicals, enhancing their viability for degradation of numerous organic compounds [1,17,36].

It is important to note that TiO₂ exhibits polymorphism, and its most common phases are anatase, rutile and brookite (Fig. 6). All three phases are comprised of TiO₆ octahedra, where each Ti⁴⁺ cation is coordinated with six O²⁻ anions but are displayed in different patterns inside the crystal. In the case of anatase and rutile, both adopt a tetrahedral crystal system, but anatase TiO₆ octahedra are significantly distorted and each octahedron is connected to eight other octahedrons (four sharing edges and other four sharing corners), whereas rutile octahedra shows a slight orthorhombic distortion and each octahedron is in contact with 10 other octahedrons (two sharing edges and eight sharing corners). The brookite phase crystallizes in orthorhombic system, in which octahedra also share edges and vertices [17,38].

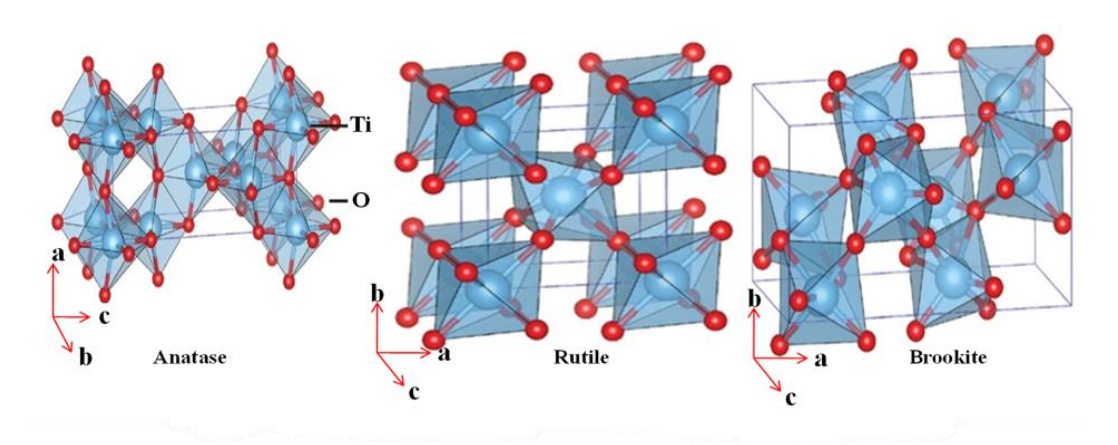


Figure 6: Representation of crystal structures of TiO₂ polymorphs - Adapted [39]

Even though all of the discussed TiO₂ polymorphs present photocatalytic properties under UV light, photocatalytic activity and general viability greatly varies in each phase. Firstly, brookite is widely considered to be the least favorable phase for photocatalysis, since not only does it have the largest bandgap (~3.4 eV), but it is also notoriously difficult to synthesize brookite based photocatalysts with high purity and surface area. Although rutile is much easier to synthesize, when compared to brookite, and has the narrowest bandgap of the polymorphs (3.0 eV), it usually presents significantly less photocatalytic activity than anatase, which, in turn, is the preferred phase for TiO₂-based photocatalysts [40].

The reason for the disparity of photocatalytic activities between anatase and rutile is mainly due to the type of electronic transition that occurs during the recombination of photogenerated e-/h+ pairs. If the top of the valence band and bottom of the CB have the same electron momentum, a direct transition occurs, where the electron returns to the VB and a photon is emitted. However, if the maximum energy of the VB and minimum energy of the CB have different electron momentum, an indirect transition occurs, and a phonon is released in addition to a photon. Rutile is a direct bandgap semiconductor and so only a photon is emitted upon recombination of charge carriers. However, in the case of anatase, a phonon-assisted transition takes place during recombination, and thus, electrons in the CB cannot recombine directly with photo generated holes, which, in turn, increases the e-/h+ pair lifetime and enhances photocatalytic activity [41].

Regardless of the polymorph used for photocatalysis, pure TiO₂ photocatalysts suffer from two major drawbacks: (i) wide bandgaps (3.0 – 3.4 eV), which requires UV-light irradiation to promote photo-induced reactions and (ii) high recombination rate of e-/h+ pairs, effectively limiting their applications. Given these intrinsic disadvantages of TiO₂, numerous modification strategies have been developed to promote visible light sensitization of TiO₂-based photocatalysts and to delay charge carrier recombination rates [39,42].

It's worth noting, however, that anatase and rutile polymorphs, when combined together, present a synergistic effect, which often result in higher photocatalytic performance than both pure polymorphs. A widely known photocatalyst is Degussa TiO₂ P25, which contains rutile and anatase in roughly 1:3 ratio. TiO₂ P25 often presents excellent photocatalytic activity under UV light due to the greatly reduced charge carrier recombination rates, although some authors present different mechanisms for this phenomenon [40].

2.1.3 TiO_2 Modification Strategies and Visible Light Sensitization

Bulk doping is one of the most well know modification strategies for visible light sensitization and photocatalytic activity enhancement of titania and other semiconductors. The doping process is based upon the deliberate introduction of metal or non-metal atoms, called dopants, into the structure of TiO₂, which can

occur either substitutionally, by substituting Ti⁴⁺ or O²⁻ in their original position, or interstitially, if the atomic radius of the dopant is small enough. The doping process may generate additional impurity energy levels within the TiO₂ bandgap which may act as an electron donor or acceptor, depending on its valence. These additional energy levels effectively reduce the energy required for electronic transitions, which in turn, may allow for visible light absorption [39,43].

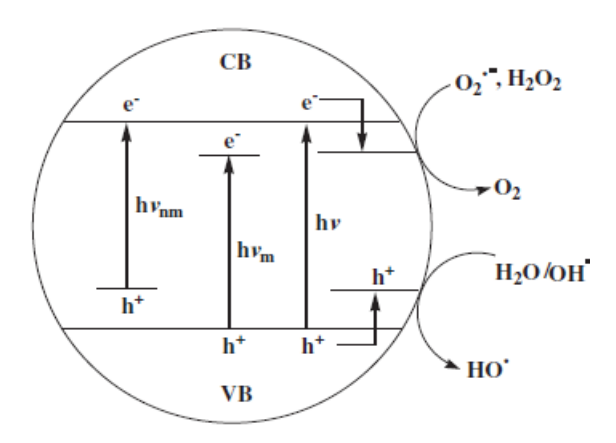


Figure 7: Schematic illustration of impurity energy levels of doped semiconductor [44].

Another viable strategy for visible light sensitization and reduced charge carrier recombination, is the formation of TiO₂ heterojunctions, which are, by definition, the coupling of titania and a different material, such as a metal or another semiconductor, or an organic compound, through interface sharing [45]. Many types of heterojunctions exist, each with their own mechanisms to enhance photocatalytic activity of titania.

Heterojunctions based on interaction between TiO₂ with metals have been extensively reported for photocatalytic purposes and are also known as Schottky junctions. In these heterojunctions, a potential barrier, known as a Schottky barrier, between the metal and the semiconductor is formed and the metal acts as a trapping center for photogenerated electrons or holes [45,46]. Conversely, the formation of TiO₂-based Schottky junctions with nanometric noble metals, such as Au, Pt and Ag, is susceptible to Surface Plasmon Resonance (SPR) phenomena, when irradiated with light. SPR occurs when surface plasmons - collective oscillations of free electrons on the surface of the metal – resonate with the electric component of an electromagnetics wave. In this context, the SPR phenomenon allows for free

electrons from the metal to be injected into the CB of the semiconductor and potentially participate in reduction reactions to degrade pollutants [39,46].

A widespread type of TiO₂-based heterojunctions is the coupling of titania with another semiconductor. These heterojunctions can be classified as three major types (I, II, and III), based on the position of VB and CB of each semiconductor involved.

In type I heterojunctions, a semiconductor with a smaller bandgap is coupled with another of a larger bandgap. Upon light irradiation, photogenerated charge carriers at the semiconductor with the largest bandgap migrate to the VB and CB of the other, leading to charge accumulation.

Type II heterojunctions consist of two semiconductors with interleaved band positions, where electrons transfer to the semiconductor with the lowest CB and holes migrate to the semiconductor of the highest VB.

Finally, in type III heterojunctions the relative positions of VB and CB of the semiconductors do not allow for any interaction and an intermediate, such as a metal particle, is needed. [45,46,47]

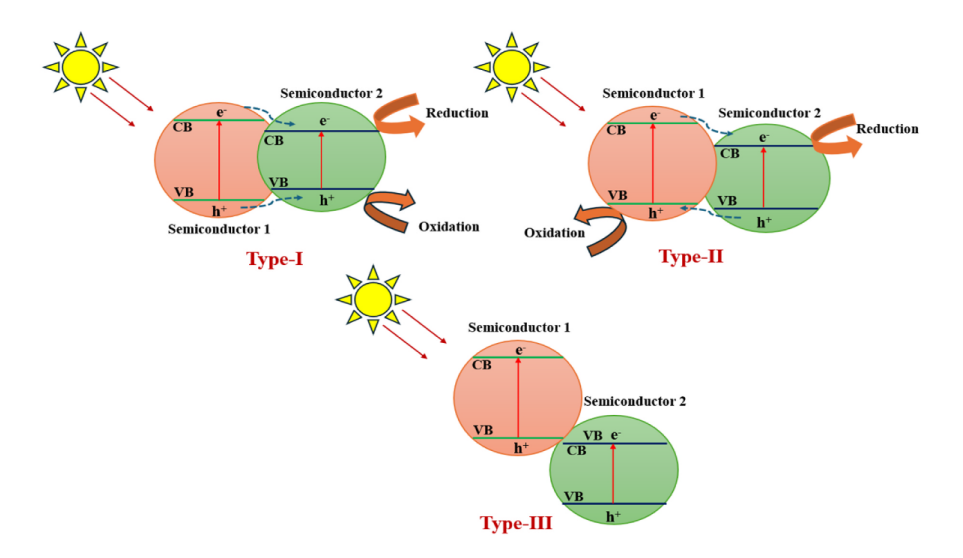


Figure 8: Charge transfer mechanism in the three main types of heterojunctions [47]

Another promising, but less explored alternative, for visible light sensitization of TiO₂ is the formation of a Ligand to Metal Charge Transfer Complex (LMCT). In this approach, the surface of titania is coated with an adsorbate, usually organic

chelating ligands, such as acetylacetone, maleic acid or EDTA. LMCT sensitization mechanism is given by the photoexcitation of electron from the ground state of the adsorbate (HOMO) directly to the CB of the semiconductor, as illustrated in Figure 9.

It is worth noting that, although similar in principle, dye sensitization mechanism differs from LMCT's, as it involves photoexcitation of electrons from LUMO of the organic compound directly into the CB of the semiconductor. Furthermore, in this case, the adsorbate (dye) is also the target compound for photodegradation [48,48,36].

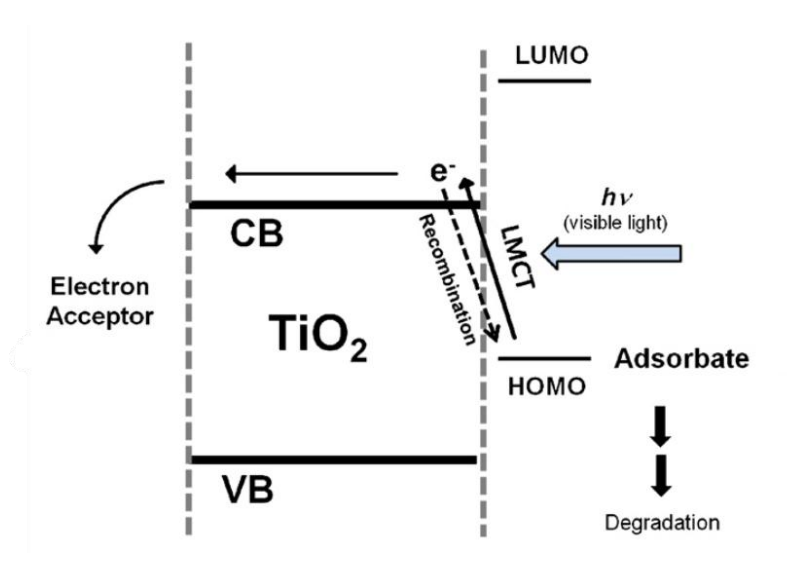


Figure 9: Visible-light sensitization of TiO₂ mechanism through LMCT complex [49].

2.2 Floating Photocatalysts

Despite the potential of heterogeneous photocatalysis for environmental remediation applications and all the discussed modification strategies to promote visible light sensitization and delayed charge carrier recombination rates, some practical aspects must be highlighted. Generally, photocatalysts are usually used in the form of nanometric or submicronic powders, to maximize surface area and, consequently, enhance photocatalytic performance. However, some issues arise from the use of fine powders in aqueous medias, such as generation of secondary

pollution and difficult recoverability and reusability of the photoactive material. Therefore, it is often viable to support photocatalyst particles onto a suitable matrix, to minimize or even prevent these drawbacks. The viability of the supporting material depends on several different factors such as guaranteeing a high surface area, good affinity (adhesion) to the active phase, good chemical stability and optical transparency to the wavelength region of the active phase [50,51,52]. The focus of the present work is on a specific type of supported photocatalysts with floating capabilities, which may present certain advantages over powder photocatalysts dispersed in the bulk of the solution.

The usage of low density and/or porous materials as a framework for immobilizing photocatalyst powder usually generates a composite material with floating capabilities. These composites may be considered as a subclass of supported photocatalysts, known as floating photocatalysts, which not only improve recoverability of photocatalyst powder, but also, according to some authors, present certain advantages over their non-floating counterpart. For instance, since floating photocatalysts remain on the surface of aqueous media, light harvesting is more efficient. Moreover, in certain scenarios both agitation and post treatment recovery of active phase may not be required, resulting in decreased operational costs. Finally, due to direct contact with water/air interface, photocatalytic performance of floating photocatalysts may also be maximized through production of more oxidizing species [53].

Numerous floating substrates may be used as a photocatalyst support; the most notable ones being perlite (vitreous volcanic rock), cork (from bark of oak trees), vermiculite (porous silicate), glass microbeads, graphite and varied polymers.

Some relatively recent studies highlight the excellent photocatalytic performance of floating photocatalysts for degradation of contaminants in aqueous media. For instance, Sboui *et al.* (2017) prepared a TiO₂-PANI composite supported on cork, by mixing the two in a vinyl binder solution. Photocatalytic activity was evaluated in a reactor containing 100 mL of 15 mg L⁻¹ dye solution and 1 g L⁻¹ of the composite. The reactor was irradiated with sunlight for a period of 4 h and a maximum degradation > 95% of the organic dye was obtained, being vastly superior to the non-supported TiO₂-PANI composite [54]. However, depending on the

particle immobilization method onto the floating framework, a decrease in photocatalytic activity may be observed, as evidenced by Hosseini *et al.* (2007). In that study, TiO₂ was immobilized onto perlite granules, *via* preparation of a titania and perlite slurry. Photocatalytic tests were performed in a 200 mL falling film micro-reactor, containing 1 mmol L⁻¹ of phenol and 11 g L⁻¹ of the floating photocatalyst, which was irradiated with 80 and 125 W UV lamps. According to the authors, the perlite/TiO₂ composite had a slight decrease in photocatalytic conversion of phenol when compared to pure P25, however it allowed for easy photocatalyst recuperation and water recirculation in the reactor [55].

Among the mentioned substrates used for floating photocatalysts, polymers are of particular relevance, as not only are many of them extremely lightweight, but also allow for formation of a porous framework; they have generally good durability under certain conditions and are usually hydrophobic, allowing for accumulation of contaminants on their surface. Additionally, polymer matrices may also be produced from recycled waste-based materials. The most used polymers for this purpose include, but are not limited to, polyethylene, polypropylene, polyurethane, polypyrrole and polystyrene [50]. The latter is particularly promising due to its broad availability and low recyclability [20]; hence it was chosen as the focus of the present study.

An extremely important aspect of polymer-based floating photocatalysts is the technique used for the photocatalyst immobilization onto a polymeric framework, as not only does each methodology has its own advantages and disadvantages but also has a direct impact on the dispersion of the photocatalyst as well as on the morphology of the composite.

Some of the methods include surface coating, sol-gel dip coating, hydrothermal treatment and phase inversion methods. Surface coating relies on a pretreatment of the target substrate, to ensure particle adhesion, followed by slowing dipping it into a dispersion or slurry loaded with photocatalyst powder. Solgel dip coating follows the same principle, only that the supporting material is inserted into a precursor solution during sol-gel synthesis of the photocatalyst. Both techniques, although simple and unexpensive, require a thermal resistant substrate if calcination is to be performed, which is usually not the case of polymers. In the hydrothermal treatment, on the other hand, both the photocatalyst and the substrate

are inserted into a heated and pressured vessel, in the presence of a proper solvent, as the powder is dissolved and deposited into the support. Although this method allows for high purity and low agglomeration, the supporting material needs to be resistant to both high temperature and pressure, severely limiting its applications with polymers [51,56].

Due to the drawbacks of the aforementioned techniques, many authors rely on phase inversion techniques or solvent casting methods for photocatalyst immobilization onto polymer substrates. Solvent casting is a very simple method where the polymer is dissolved by a suitable solvent, forming a polymeric solution, to which the photocatalyst is then added. After homogenization, the remaining solvent is dried, usually at room temperature and a monolithic composite is obtained [15].

Phase inversion methods are divided mainly into Thermally Induced Phase Separation (TIPS) and Non-solvent Induced Phase Separation (NIPS). Both methods share similar first steps to the solvent casting method, as the polymer is first dissolved into a solvent, followed by the addition of photocatalyst. However, in TIPS methodology the solvent is removed by freeze-drying the dispersion [20,57,58]. This method is used for formation of low weight and porous composites.

On the other hand, in NIPS methodology a polymer solution, which may contain the photocatalyst powder, is induced to separate into two distinct phases with the addition of a non-solvent [59,60,61]. This technique is usually applied for formation of porous, thin polymeric films, but it was unprecedently adapted for the present study, as it will be further discussed.

Another possible immobilization technique involves dispersion photocatalyst powder in a solution of the precursors of the desired polymer and, subsequently, promoting polymerization. Depending on how polymerization occurs, this method usually yields foamy composites with homogenous dispersion of active phase [62]. However, it requires more reactants, fine tuning of polymerization and impedes usage of recycled material.

When it comes to general use of polymers as substrate for floating photocatalysts, numerous reports have been made regarding them for

environmental remediation purposes, applying different techniques for photocatalyst immobilization onto polymeric frameworks.

Li *et al.* (2015), synthesized TiO₂/Polyurethane (PU) composite foam by mixing the photocatalyst into a precursor solution during polymerization of polyurethane. Prior to the immobilization onto PU, titania particles were first immobilized onto hydrophobic-pillared organic montmorillonite, which, according to the authors, would facilitate for uniform dispersion of titania in PU foam. Photocatalysis experiments were conducted in a batch column reactor containing 500 mL of Bisphenol A (BPA) solution (20 mL L⁻¹) along with 1 g of photocatalyst under UV light irradiation (60 W). According to the authors, all photocatalysts provided a degradation efficiency above 50% after 120 min, and the composite containing 40% of active phase yielded the best results, with a total conversion of 83% of BPA [62].

Han and Bai (2009), prepared TiO₂/polypropylene floating composites by mixing titania powder and polypropylene granules, in a hydrothermal reactor, at 150 °C for 10 h. Photocatalytic activity was evaluated through photodegradation of methyl-orange, in a beaker containing 50 mL of a 15 mg L⁻¹ solution of the contaminant. Around 100 granules of the composite were added into the solution, which was irradiated with a 150 W UV-Vis light, for 4 h. A maximum degradation efficiency of 65% was obtained [63].

Magalhães *et al.* (2011) prepared TiO₂ P25 particles embedded in low density polyethylene substrates, with different photocatalysts loadings, through solvent casting method. Photodegradation tests were performed in a 400 mL reactor with 100 cm² surface area, containing 200 mL of a 0.16 mmol L⁻¹ methylene blue solution and up to 1 g of photocatalyst, with solar light irradiation during 4 h. The authors reported complete removal of contaminant and also concluded that increasing photocatalyst loading leads to diminishing increments to photocatalytic activity, as particles start to agglomerate [64].

Table 1. Summary of the studies related to polymer-based floating photocatalysts for environmental remediation.

Source	Floating	Immobilization	Experimental	Removal
Source	Photocatalyst	Technique	Conditions	Efficiency
			$[BPA]_0 = 20 \text{ mg L}^{-1}$	
[62]	T:O. /M+/ DII	In situ Polymerization	Photocat = $1 g$	83% after 120 min
[~-]	TiO ₂ /Mt/ PU		V = 500 mL	
			60 W UV-light	
			$[MO]_0 = 15 \text{ mg L}^{-1}$	~65% after 4h
[63]	Ti'O /DD	Hydrothermal	V = 50 mL	
լսոյ	TiO ₂ /PPy	Method	Photocat. = $15 - 20 \text{ mg}$	
			150 W Xenon Lamp	
		Solvent Casting	$[MB] = 0.16 \text{ mmol } L^{-1}$	100% after 240 min
[64]	T10 /P7		Photocat. = 1 g	
[04]	TiO ₂ /PE S		V = 200 mL	
			Sunlight	
	1000	In situ Polymerization	$[MO]_0 = 10 \text{ mg L}^{-1}$	
[65]			Photocat. = $0.1 g$	88% in 60
լսոյ			V = 100 mL	min
			300 W Xenon Lamp	
		$[MO]_0 = 4 \text{ mg L}^{-1}$	80% after	
	PEI-g-C ₃ N ₄ Solvent Casting		Photocat. = 0.1 g	68 h with stirring. 55% after
[66]		Solvent Casting	V = 50 mL	
				11 W Table Lamp
	TiO ₂ -PUF Ultrassonic mixing of PUF and TiO ₂ dispersion		$[Cr^{6+}] = 10 \text{ mg L}$	
(<i>(</i> = 1)			40 pieces of TiO ₂ -PUF composite	83.6% and 97.4% of
[67]		and TiO ₂	$[RhB] = 10 \text{ mg L}^{-1}$	Cr ⁶⁺ and RhB after
		V = 20 mL	150 min	
			Sunlight (1000 W m ⁻²)	

The particular use of polystyrene (PS) as floating substrate for photocatalyst immobilization has been reported in a few previous studies.

de Assis *et al.* (2018) synthesized PS/SnO₂ composites from waste-based materials by the TIPS method. Photocatalytic tests were carried out by monitoring photodegradation of Rhodamine B under 45 W UV light, while varying the concentration of both photocatalyst and contaminant. While the dimensions of the photocatalytic chamber were described, no information of the volume of contaminant solution, nor the mass of the composite were provided. The authors concluded that the PS/SnO₂ composites prepared by the TIPS method were capable of almost complete removal of Rhodamine B, while also presenting high reusability [18].

Singh *et al.* (2014) immobilized Ag⁺ doped TiO₂ nanoparticles both into and onto PS films *via* solvent casting method. Photodegradation tests were performed in a Petri dish containing 50 mL of a 5 mg L⁻¹ solution of methylene blue, where the floating composite films (photocatalyst equivalent of 1 g L⁻¹) were deposited upon. The authors report photodegradation efficiency of over 94%, under UV light (100 W) irradiation for a period of 5 h [68].

Table 2. Summary of studies that applied PS-based floating photocatalysts for environmental remediation purposes.

Source	PS Floating Photocatalyst	Immobilization Technique	Experimental Conditions	Efficiency
			$[RhB]_0 = 1.0 \times 10^{-5}$ mol/L [photocat.] = 0.4 g	~100% after
[18]	PS/SnO ₂	TIPS	L-1 Three 15 W UV	~100% after 70 min
			lamps $[MB]_0 = 5 \text{ mg L}^{-1}$	
[68]	Ag ⁺ -TiO ₂ /PS	Solvent Casting	[photocat.] = 1 g L ⁻	94% after 5 h
			V = 50 mL	

			100 W UV light	
			$[MB]_0 = 10 \text{ mg L}^{-1}$	
			$[Phenol] = 50 \text{ mg}$ L^{-1}	~100% of MB and
[69]	N-TiO ₂ /PS	Solvent Casting	Photocat. = $0.2 g$	72% pf phenol, after
			V = 30 mL	180 min
			Three 8 W visible-light lamps	
			[MB] = 15 - 105	
			mg L ⁻¹	~100% of
[70]	TiO ₂ -PS	Thermal Immobilization	Photocat. = $0.3 - 0.7 \text{ g}$	MB (15 mg L ⁻¹) after 150 min
			UV-A lamp	

Based on the works cited so far, some key points and few contradictions were reported by some of the authors that need to be highlighted. First and foremost, nearly all the referenced works on polymer-based floating photocatalyst affirm that agitation of reaction media is dispensable. However, in most reported cases, what makes stirring dispensable is not the use of a floating photocatalyst by itself, but the use of a low-volume (<100 mL) or shallow reaction media. These conditions not only present difficult scalability and real-world application but may also artificially overestimate the photodegradation rate. Moreover, a notable contradiction between some reports, that has yet to be explained, regards the specific surface area of the composites. As shown in Table 3 some authors report that supporting powder photocatalysts onto a porous polymeric support, such as PS, results in an increase of specific surface area, claiming that the polymeric matrix reduces particle agglomeration. However, some other authors report the contrary, attributing the reduction of specific surface area to particle occlusion.

Table 3: Reported specific surface areas of polymer-based floating photocatalysts.

Source	Immobilization	Photocatalyst/	Specific Surface	
Source	Method	Support	Area (g m ⁻²)	
[18]	TIPS	SnO ₂ (700 °C)	15.2	
[10]	111.5	PS(2.5)/SnO ₂ (5)-700	48.7	
		g-C ₃ N ₄	15.6	
[65]	In Situ Polymerization	Ag/g - C_3N_4	23.8	
	·	$PPy@Ag/g-C_3N_4\\$	39.8	
	In Situ	ZnO	4.9	
[71]	Polymerization	PPy	24.4	
	1 ory menzacion	PPy-ZnO (25:1)	48.0	
		TiO ₂ -P25	40	
[62]	In Situ Polimerization	PU	5	
		T@Mt/PU-4	17	
		TiO ₂ -P25	50	
		LDPE	0	
[64]	Solvent Casting	TiO ₂ (30)/LDPE	1	
		TiO ₂ (68)/LDPE	2	
		TiO ₂ (82)/LDPE	4	
	Solvent Casting	ZnO	5	
		TiO_2	47	
[72]		PS (pellets)	0.03	
		2% ZnO-PS	0.2	
		1.1%TiO ₂ -PS	0.2	

Furthermore, some knowledge gaps have been identified. Different studies claim that photocatalytic degradation of PS in aqueous media is not only possible, but also a viable way to remove microplastics from water or degrade PS altogether [73,74,75]. Based on these reports, the chemical stability of PS-based floating photocatalysts is questionable and may be compromised during photocatalysis. However, as of the time of writing the present work, there are no studies on the photochemical stability of PS-based floating photocatalysts. Moreover, there are no reports on the use of TiO₂-ACAC CTC, a photocatalyst developed by our research group, with any type of support whatsoever.

This research work aims to study, for the first time as the author is aware, the photocatalytic activity of PS/TiO₂-ACAC nanocomposites in the degradation of an antibiotic in bulk aqueous media, prepared by NIPS and TIPS methods. Along with photocatalytic performance, the study also expected to contribute to better understanding of the aforementioned issues with contradictory reports in the literature, principally regarding the (i) surface area of polymer-based floating photocatalysts, (ii) experimentally favorable conditions for photocatalysis, which do not reflect real-world applications and (iii) the uncertain photochemical stability of the PS support.

Objectives

3.1 General objective

The present work aims to evaluate floatable photocatalysts based on waste polystyrene and TiO₂-ACAC charge transfer complex nanoparticles for the photodegradation of an antibiotic molecule, such as tetracycline.

3.2 Specific objectives

- Synthesize TiO₂-ACAC charge transfer complex nanoparticles and immobilize them onto a polystyrene floatable support.
- Thoroughly characterize both the non-supported and supported photocatalysts through various techniques.
- Acquire and compare the data on the photocatalytic performance of both the supported and non-supported materials for the photodegradation of tetracycline.
- Evaluate scientific feasibility of such a floating photocatalyst and contribute to the better understanding of the contradictions present in literature, such as photochemical stability of PS-based floating photocatalysts.

Recycled Polystyrene-based TiO₂-Acetylacetone Floating Photocatalysts for Degradation of Antibiotics

4.1 Introduction

Over the past century, accelerated urbanization and industrialization processes took place around the world, drastically changing the relationship between humans and the environment. Due to continuous unsustainable practices, numerous environmental problems have emerged, with the pollution of aquatic environments being among them. An alarming quantity of toxic and/or environmentally hazardous residues, originating from residences, factories, and agricultural and livestock activities, are inappropriately released in aquatic media to this day, which pose an immediate threat to various ecosystems and, possibly, to human health [1,2].

A new class of pollutants, known as emergent contaminants, which are commonly found in wastewater residues mostly comprised of pesticides, fertilizers, dyes and pharmaceuticals, have been the subject of various studies due to their potential toxicity and chemical stability, making them susceptible to bioaccumulation and biomagnification processes [3,4]. Emergent pollutants are also known for being particularly hard to degrade and abate through conventional wastewater treatment processes. Therefore, new sustainable techniques for the removal of these contaminants must be developed before more severe environmental impacts become a reality [5].

Regarding emergent contaminants, numerous removal and/or degradation techniques have been reported, including the use of adsorbent materials, nanofiltration membranes, precipitation and coagulation [8,9,10]. Among these techniques, Advanced Oxidation Processes (AOPs) are particularly promising due to the possibility of degradation and abatement of various types of organic

pollutants, often to the point of complete mineralization [11,12,13]. Amidst the many AOP techniques, heterogenous photocatalysis has been a recurring topic for environmental remediation, due to high pollutant conversion rates, low cost and, in theory, uncomplicated application. This method is based on the promotion of photo-induced oxidation reactions of pollutants on the surface of a semiconductor acting as photocatalyst. Moreover, photocatalysis becomes more relevant if visible light, or even sunlight, can be used to promote photodegradation reactions.

Heterogeneous photocatalysis has been widely studied as a means of environmental remediation of organic pollutants. Although many semiconductors, such as WO₃, SnO₂, CdS and ZnO, to mention some of them, may act as a photocatalyst, TiO₂-based materials are undoubtedly the preferred due to their nontoxicity, high chemical stability, relatively low cost and broad availability [1,14,36,66,76,77]. Moreover, anatase is usually the preferred polymorph of TiO₂, since it presents higher photocatalytic activity due to phonon-assisted recombination of e⁻/h⁺ pairs [40]. However, even in the anatase phase, TiO₂ suffers from two major drawbacks: (i) wide bandgaps (3.2 eV), which requires UV-light irradiation to promote photo-induced chemical reactions, (ii) high recombination rate of e⁻/h⁺ pairs [15,16].

To counteract these drawbacks, several surface modification approaches of TiO₂-based photocatalysts have been proposed, including noble metal and non-metal doping, heterojunctions and defect engineering [1,45,78]. A relatively new alternative and, therefore less discussed, is the formation of Ligand-to-Metal Charge Transfer Complex (LMCT) by coupling small organic molecules to the surface of the titania and some other photocatalysts [16,48,49]. The LMCT mechanism is based on the promotion of electrons from the HOMO of the organic molecule into the CB of the semiconductor, enabling the semiconductor to produce Reactive Oxygen Species (ROS), namely hydroxyl (.OH) and superoxide (.O₂-) radicals. Among the possible ligands, Acetylacetone (ACAC), an oxygen based bidentate ligand, which was originally used by Scolan and Sanchez to control hydrolysis and condensation reaction rates during sol-gel synthesis of titania nanoparticles, has been reported to promote light sensitization when used in excess [79].

Almeida *et al.* reported the influence of calcination temperature on the physical and photocatalytic properties of TiO₂-Acetylacetone (TiO₂-ACAC) charge transfer complex [16]. The authors found that calcination at 300 °C resulted in a high surface area crystalline nanopowder, capable of absorbing visible light with significantly superior photocatalytic performance over the materials obtained at higher calcination temperatures. On the other hand, Gil-Londoño *et al.* studied the influence of extrinsic point defects, such as oxygen vacancies, in TiO₂-ACAC system for tetracycline degradation in aqueous media [78]. It was reported that, although the presence of oxygen vacancies improves visible light sensitization, high concentrations of single electrons trapped in oxygen vacancies (SETOV) allow trapped electrons to migrate between defects, due to their proximity, resulting in increased charge carriers' recombination rates, thus, high concentrations of oxygen vacancies likely do not contribute to the increase of photocatalytic activities in TiO₂-ACAC system.

Although certain modification strategies of neat and chemically pure TiO₂ may prove effective to compensate for the inherent disadvantages of TiO₂- based photocatalysts, the issue of how it is implemented in the reaction medium remains. TiO₂, as well as other photocatalysts, are usually used in the form of submicronic or nanometric powders, to maximize surface area and enhance the photocatalytic reaction rates [29]. Even though effective from photocatalytic activity point of view, this approach also presents disadvantages, for instance, technically difficult and/or costly recuperation of fine powder from reaction medium and, consequently, impractical reuse of the photocatalysts [53].

An alternative to the direct insertion of fine powders into the reaction medium is to immobilize photocatalysts onto a suitable matrix, as a support. Ideally, the supporting material must be chemically and photochemically inert, especially in the presence of light irradiation and ROS, ensuring, also, good adhesion of nanoparticles onto the matrix and presenting high surface area [52]. In this regard, polymers, more specifically PS, appear to be a good candidate for supporting material, since potentially meets the requirements of a good support material, but it also may be prepared from PS waste, increasing the applications of recycled PS [18].

Due to its extremely low density, photocatalysts supported onto a PS matrix are usually classified as a floating photocatalyst. This type of photocatalyst presents unique advantages such as increased sun light harvesting, high surface oxygenation of the photocatalyst, possibly leading to increased concentration of .O₂⁻ radicals, simple separation from aqueous media and reusability [50,51,52]. Furthermore, as highlighted by Seifikar *et al.*, floating photocatalyst may prevent overexposure of the active phase to the reaction system, which can lead to increased photocatalytic activity [53].

Numerous studies have reported PS as a floating substrate for photocatalyst immobilization. For example, de Assis *et al.* successfully synthesized waste-based PS@SnO₂, through Thermally Induced Phase Separation (TIPS) method applying freeze-drying of a PS/cyclohexane/SnO₂ dispersion. The study reported an increased photocatalytic performance of PS@SnO₂ in the degradation of Rhodamine B [18].

El-Samak et al. fabricated porous PS/ZnO nanocomposites through Non-solvent Induced Phase Separation (NIPS) assisted with electro-spinning. The PS/ZnO composite fibers were subjected to photocatalytic tests in the presence of Azocarmine G dye and were capable of degrading over 85% of the contaminant in 6 h, under sunlight [80]. It is worth noting that other floating substrates have been used as support for TiO₂ based photocatalysts, including perlite, cork, fly ash and other polymers [54,81,82,83].

Although polymer-based floating photocatalysts may prove advantageous in certain scenarios, conflicting and contradictory data regarding specific areas, polymer photochemical stability and photocatalytic activity were found. For example, some authors claim that supporting photocatalyst powder in a polymeric matrix not only increases specific surface area but also reduces particle agglomeration [18,65,71]. Others, however, report the opposite, alleging that supported materials present a lower specific area due to partial or total particle occlusion [62,64,72]. Photochemical stability of the supporting polymer is also a topic of special concern since it could contribute to undesirable secondary microplastic pollution. Some studies claim polystyrene to be inert in the presence of ROS and, therefore, a suitable supporting material [68,84,85]. Conversely, some

other authors report photodegradation of polystyrene in the presence of a suitable photocatalyst [73,74,75,70].

Finally, there is an argument to be made regarding photocatalytic performance of polymer supported photocatalysts. While many authors report an increased photocatalytic activity relative to the photocatalyst powder counterpart, most of these results are derived from the photocatalytic systems with very low volume (< 100 mL), which not only have limited applicability, but also may provide artificial favorable conditions for photocatalysis with floating substrates [66,67,68,69].

Given the context related to visible light sensitization of titania through LMCT complexes and to floating photocatalysts, the present study aims to test, for the first time, the photocatalytic performance of the TiO₂-ACAC charge transfer complex supported on waste based polystyrene matrix on the degradation of an antibiotic (tetracycline). The immobilization of TiO₂-ACAC nanoparticles onto PS matrix has been performed by the previously reported TIPS method and an unprecedent adaptation of the NIPS method. Furthermore, the supported photocatalyst were directly compared to its non-supported counterpart. In addition, scientific feasibility of such a floating photocatalyst has been evaluated and contribution to the better understanding of photochemical stability of PS-based floating photocatalysts has been offered.

4.2 Materials and Methods

4.2.1 Sol-Gel Synthesis of TiO₂-Acetylacetone Charge Transfer Complex

The synthesis of TiO_2 -ACAC charge transfer complex was carried out by the Sol-Gel method, as described in previous works of our research group maintaining a molar ratio [ACAC]/[TiO_2] = 2 [16,86,78].

Firstly, a mixture of 100 mL of ethanol (Sigma-Aldrich, ~99%) and 20 mL of Acetylacetone (Sigma-Aldrich, ~99%) was prepared and magnetically stirred until a yellow and homogeneous solution was achieved. Next, 30 mL of Titanium Isopropoxide (Sigma-Aldrich, ~99%) was added dropwise to the previously

prepared solution. After 40 minutes of stirring, 180 mL of a diluted aqueous solution of HNO₃ (0.015 mol L⁻¹) was slowly added dropwise to the mixture, to promote hydrolysis and condensation reactions. The resulting solution was then heated to 60 °C and kept under constant stirring until a yellow/orange gel was formed.

The gel was left drying in a petri dish overnight at room temperature, to remove the excess of water and solvent. The partially wet cake was then dried at 100 °C in a laboratory oven for 24h and orange bulky crystals of TiO₂-ACAC xerogel were obtained. The material was then manually milled with mortar and pestle for 20 min and a fine orange/yellow powder was obtained.

Regarding the use of TiO₂-ACAC CTC for pollutant degradation, the works of Almeida *et al.* and Gil-Londoño *et al.* reported high photocatalytic performance of materials calcined at 300 °C and 270 °C, respectively. As such, the resulting xerogel (denoted as TiO₂-ACAC) would undergo two distinct, but similar, thermal treatments. A portion of the xerogel was calcined at 270 °C, for 2h, while another portion was calcined at 300 °C, for 3h, which were denoted as TiO₂-ACAC270 and TiO₂-ACAC300, respectively. These materials would undergo a series of photocatalyst tests, and the one with the highest photocatalytic performance was chosen for immobilization onto PS matrix to form nanocomposites.

AEROXIDE® TiO₂ P25, a commercial photocatalyst currently supplied by Evonik GmbH with anatase and rutile crystalline structure, has been used as reference in some of the photocatalytic experiments.

4.2.2 Photocatalysts Immobilization onto Recycled Polystyrene Matrix

4.2.2.1 Non-solvent Induced Phase Separation (NIPS)

As previously discussed, NIPS methodology is usually applied to the synthesis of polymeric membranes, which may also be supported with photocatalytic materials and used in membrane reactors.

The present work uses a novel approach to NIPS technique, as an adaptation of the methodology used by Bianco *et al.* to produce polystyrene beads, while also simultaneously using a nanoparticle immobilization technique, similar to the one used by Bhattacharyya *et al.* [59,60]. One major modification of the aforementioned works is that no surfactant was added to the polymeric solution, since eventual failure to remove surfactant molecules from the polymeric matrix could result in their degradation during photocatalytic tests [87].



Figure 10: PS/TiO₂-ACAC composite beads prepared by NIPS methodology.

The adapted NIPS route used waste polystyrene foam (StyrofoamTM cups), previously washed and crushed as the polymeric starting material. The photocatalyst immobilization started by dissolving the polystyrene foam in N,N-dimethylacetamide (Vetec, 99%) to form a 10% (m/v) polymeric solution. After approximately 10 min of stirring at 50 °C, 5 mL of the polymeric solution was transferred to a beaker and photocatalyst powder (TiO₂-ACAC300 or TiO₂-P25), corresponding to 30% or 50% of total composite weight, was added to the mixture. A uniform dispersion of photocatalytic nanoparticles in the polymeric solution is formed after around 10 minutes of stirring, judging by its homogenous color and absence of macroscopic agglomerates The mixture is then transferred dropwise to a beaker containing 400 mL of distilled water under constant stirring, so that the phase separation through the solvent exchange can occur, resulting in small irregular beads of polystyrene containing TiO₂-ACAC300 or TiO₂-P25 (Figure 10).

The composite beads are removed from water by vacuum filtration and are thoroughly washed with approximately 300 mL of distilled water to remove any residual solvent and weakly adhered nanoparticles. Finally, the beads are dried in an oven at 70 °C for 4 h. The materials prepared by this route were identified as PS-NIPS/TiO₂-ACAC300 (30% and 50%) and PS-NIPS/P25 (30% and 50%). Multiple batches of composite beads have been prepared.

4.2.2.1 Thermally Induced Phase Separation (TIPS)

The TIPS process for the synthesis of photocatalytic foams was performed through a slight modification of the methodology described by de Assis *et al.* (2018) [18]. In the present work, PS composites were obtained from polymeric solutions containing 10% (m/v) of PS and photocatalysts loading percentages were 30% and 50% (m/m) of the total composite mass.



Figure 11: PS/TiO2-ACAC composite prepared by TIPS methodology

For this route, a 10% (m/v) polymeric solution of polystyrene was prepared by dissolving the crushed StyrofoamTM cups (same as applied in NIPS route) with cyclohexane (Cinética, 99%), in the right proportions. After approximately 20 min of stirring at 50 °C, 5 mL of the homogenous polymeric solution is then transferred to a beaker and 220 (367) mg of the photocatalyst, which roughly corresponds to 30% (50%) of the composite's total mass, was added into the mixture. The mixture was then thoroughly stirred for around 10 min, until a uniform dispersion was formed, which was then taken to a freezer at -5 °C. After 1 h, the frozen mixture

was taken to a freeze-dryer (Labconco®, FreeZone 2.5 Liter) and dried in vacuum for 90 min, at -50 °C. The resulting materials were disc-shaped polymeric supports, containing TiO2-ACAC300 nanoparticles and were identified as PS-TIPS/TiO₂-ACAC300 (30% and 50%), as shown in Figure 11. Multiple batches of the PS-TIPS/TiO₂-ACAC300 based composites have been prepared.

4.2.3 Characterization Techniques

The crystal phase of the TiO_2 -ACAC nanoparticles were determined by X-Ray Powder Diffraction (XRPD), using a Bruker D8 Advance diffractometer, operating under Cu K_{α} radiation. Data were acquired in the range of 20° to 80° (20), at a step size of 0.02° and an acquisition time per step of 2 s. Le Bail method was used for peak fitting, through TOPAS 4.2 software, to determine phases, lattice parameters and crystallite size.

Thermogravimetry Analysis (TGA) and Differential Scanning Calorimetry (DSC) were performed in a Perkin-Elmer Simultaneous Thermal Analyzer STA 6000. In the case of non-supported photocatalysts, analyses were carried out under constant synthetic air flow (20 mL min⁻¹), at a heating rate of 10 °C min⁻¹ in the temperature range between 30 and 600 °C. For the photocatalysts supported onto polystyrene matrix, analysis was done under constant N₂ flow. The heating rate and temperature range remained the same.

Nitrogen adsorption-desorption isotherm analysis was performed for both supported and non-supported photocatalysts, using a Nova Touch LX2 surface area & pore size analyzer (Quantachrome). A 3 h pretreatment of samples was done under a vacuum of 50 mTorr, at 120 °C for powder photocatalysts and at 80 °C for the polymer supported photocatalysts, while data acquisition for nitrogen physisorption was performed at -196 °C (77 K). From the adsorption-desorption isotherms, the specific surface area (BET S.A.) of the porous materials was calculated by the Brunauer-Emmett-Teller method (BET).

Density of composites prepared by both NIPS and TIPS methods were measured by Archimedes principle. Samples were first weighed and then inserted into a graduated cylinder containing a known volume of distilled water. The displaced volume of water was used as an estimate for the composite's volume, and the density was calculated.

In order to verify if the PS matrix indeed promoted nanoparticle occlusion in NIPS and TIPS composites, a theoretical specific area (TSA) calculation was performed, which, as shown in Equation 1, is a weighted average of the areas of pure PS foam and the active phase, in relation to the mass percentage of each phase, as determined by TGA. This calculation is based on the premise that active phase encapsulation by the PS matrix did not occur. Consequently, if the experimental BET specific area of the composites is lower than the TSA, then encapsulation has occurred during nanoparticle immobilization.

$$TSA = x_{PS}A_{PS} + x_TA_T \tag{1}$$

 x_{PS} : Mass percentage of PS phase

 A_{PS} : BET specific area of pure PS

 x_T : Mass percentage of TiO₂-ACAC nanopowder

 A_T : BET specific area of TiO₂-ACAC nanopowder

Fourier Transformed Infrared Spectroscopy (FT-IR) was performed on a PerkinElmer Frontier. Samples were prepared by mixing 2 mg of photocatalyst nanopowders with 200 mg of KBr, which were then pressed at 10 bar for 2 min. Spectra wavenumber ranged between 4000 to 400 cm⁻¹, with a resolution of 4 cm⁻¹ and 16 scans.

Electron Paramagnetic Resonance (EPR) spectra were obtained in a modified commercial MiniScope400 spectrometer (Magnettech GmbH, Berlin, Germany), operating at 9.45 GHz with a field modulation of 100 kHz and amplitude of 0.2 mT. The magnetic field was generated by a Varian (9") electromagnet coupled to a Walker (Salem, USA) DC current source. Temperature of 300 K was maintained during measurements with a ESR 900 (Oxford, England) He flux cryosystem. EPR measurements of powder samples of TiO₂-ACAC, TiO₂-ACAC270 and TiO₂-ACAC300 were performed in quartz tubes. Experimental parameters include 10 mW of microwave power, field centered at 337 mT, with application interval of 10

mT, scan time of 60 s and 4096 integration points. Additional spectra simulations were obtained by Easyspin software.

SEM images of both supported and non-supported photocatalysts were acquired at a TESCAN CLARA Scanning Electron Microscope, with a FEG BrightBeam electron column, operating at 10 kV.

TEM images of photocatalysts nanopowders were acquired by a Talos F200X G2 (ThermoFisher), operating at 200 kV. Sample preparation was performed by dispersing a small quantity of TiO₂-ACAC and TiO₂-ACAC300 powders in isopropanol via ultrasonic bath, during 20 min. A minute volume of the dispersion was transferred, dropwise, to a copper grid supported with a lacey 200 mesh carbon film. After isopropanol evaporation, the sample holder, containing the retained photocatalyst particles, was inserted into the equipment.

Total Organic Carbon (TOC) analysis was performed in filtrates of dedicated experiments to verify incomplete mineralization in tetracycline photodegradation and the photo(chemical) stability of the polymeric matrix. TOC analyses were conducted in a TOC-L CNP (Shimadzu), using potassium biphthalate as analytical standard and a 0-10 mg L⁻¹ calibration curve.

TOC experiments were also performed to evaluate both physical and photochemical stability of PS matrix. Pure PS-NIPS beads, as well as the 30% and 50% NIPS composites, were added to 500 mL of distilled water with no contaminants. The amount of material added was equivalent to 1 g of PS, hence 1 g of PS-NIPS, ~1.5 g of PS-NIPS/TiO₂-ACAC300 (30%) and 2 g of NIPS/TiO₂-ACAC300 (50%) were added into the reactor, in two separate sets of tests. The first set of tests, the system was kept in the dark for 6 h, under constant agitation, and samples were taken from the reactor in 1 h intervals. In the second set of experiments, the system was kept in the dark, under agitation for 1 h. Afterwards, a 100 W visible light halogen lamp was turned on and samples were taken from the reactor in 1 h intervals, for 6h

4.2.4 Measurement of Photocatalytic Activity

Preliminary photocatalytic tests of non-supported photocatalysts were performed by photodegradation of tetracycline in an aqueous environment under visible light. The tests were carried out in a laboratory batch reactor, coupled with a DULUX D/E fluorescent lamp of 26 W power and an irradiance of 0.23 W cm⁻² (400-700 nm); a glass jacket, through which flows current water, kept the reaction medium near the room temperature when the light is turned on. The reactor was filled with 1 L of distilled water containing 200 mg L⁻¹ of photocatalyst powder, while tetracycline initial concentration was 10 mg L⁻¹, maintaining a 20:1 mass ratio of photocatalyst and pollutant. Each photodegradation test was carried out for 6 h.

After these preliminary tests, the photocatalyst with the best photocatalytic performance was selected for the photodegradation tests involving PS floating nanocomposites. Photodegradation tests were conducted with PS-NIPS/TiO₂-ACAC300 and PS-TIPS/TiO₂-ACAC300 composites. Initial TC concentration was 50 mg L⁻¹ and to keep the 20:1 photocatalysts/contaminant ratio, 1 g L⁻¹ of photocatalysts immobilized into PS matrix was used. It is important to note that the amount of photocatalyst was kept constant for each test, and therefore, different quantities of the 30% and 50% composites were used in the tests (~1.5 g and 2 g of the PS-TIPS/TiO₂-ACAC300 (30%) and PS-TIPS/TiO₂-ACAC300 (50%) composites, respectively). In addition, this batch of experiments were performed using a 100W visible-light halogen lamp, since preliminary tests using the 26W LED lamp yielded little to no photocatalytic activity, which could be due to low light harvesting of nanoparticle embedded within NIPS beads. The tests were carried out in the photoreactor with 500 mL volume and under moderate agitation.

After the addition of photocatalytic material (supported or non-supported) to the reaction medium, the system was kept in the dark until adsorption-desorption equilibrium was achieved, and only then was the fluorescent light turned on. Aliquots of 5 mL were acquired at designed time intervals, filtered using a Merck Millipore filter (0.22 μ m), transferred to a quartz cuvette and analyzed by a UV-Vis Spectrophotometer (Agilent 8453, USA). Tetracycline adsorption bands at 276 and

358 nm were monitored, and the intensity of the former one was used to calculate total photodegradation.

4.3 Results and Discussion

4.3.1 Characterization and Photocatalytic Performance of TiO₂-ACAC CTCs

X-ray powder diffraction patterns of TiO₂-ACAC, TiO₂-ACAC270 and TiO₂-ACAC300 nanopowders, shown in Figure 12, highlight the influence of calcination temperature over crystallinity of each sample. The XRPD patterns of TiO₂-ACAC xerogel presented broad and overlapping peaks, an indicative of nanometric crystallite size and presence of amorphous phase. Calcined samples at 270 and 300 °C showed narrower and well-defined peaks of the anatase phase, which are identified in Figure 12-d. No other TiO₂ polymorph was detected, as calcination temperatures used were too low to promote phase transformation to rutile, which is the thermodynamically stable phase of titania [16].

To confirm the presence of nanometric crystallites, peak fitting of the XRPD patterns was performed by Le Bail method. Mean crystallite size of TiO₂-ACAC xerogel was estimated to be 1.2 nm, while calcined materials at 270 and 300 °C presented an increase of mean crystallite size of anatase to 7.4 and 7.6 nm, respectively.

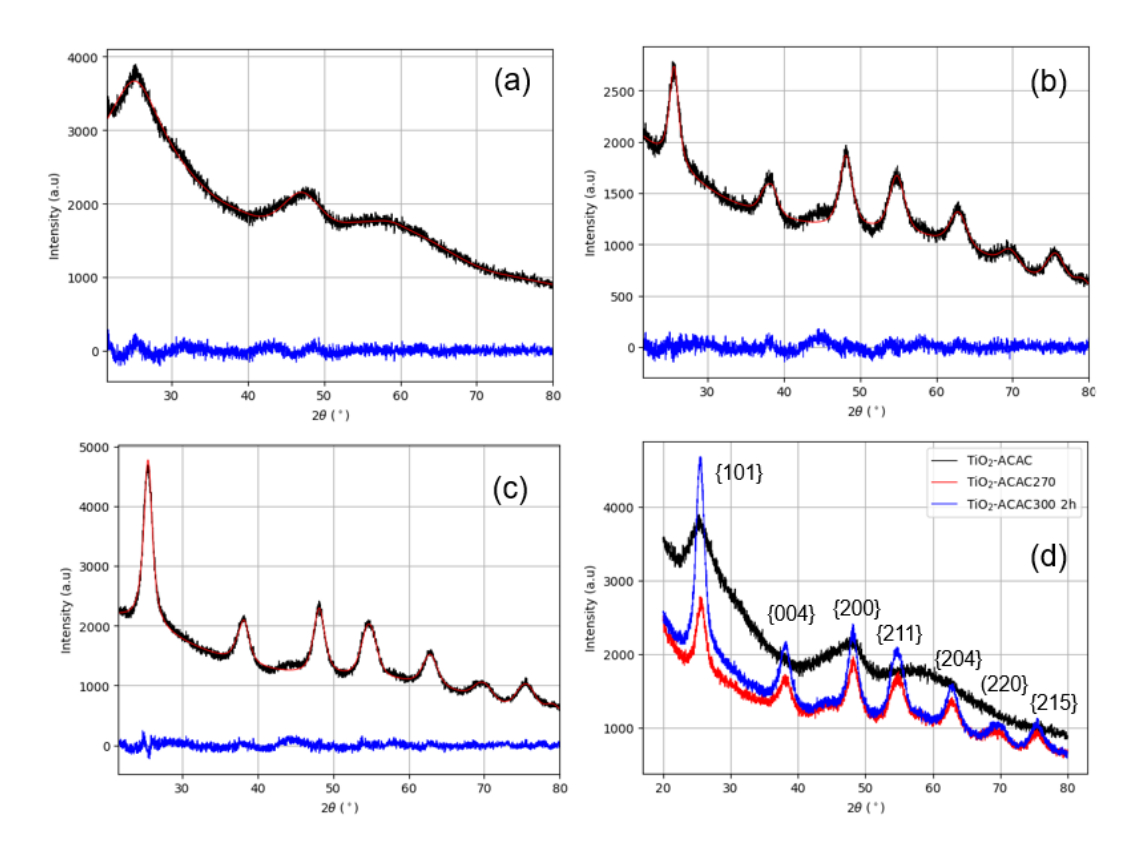


Figure 12: XRPD patterns of TiO₂-ACAC xerogel (a), TiO₂-ACAC270 (b), TiO₂-ACAC300 (c) and peak identification (d)

The N₂ adsorption-desorption curves of the as-synthesized photocatalysts (Figure 13) present vital information on pore size and distribution. Both TiO₂-ACAC and TiO₂-ACAC270 presented Type I physisorption isotherms, typical of microporous materials, without the presence of significant hysteresis. On the other hand, TiO₂-ACAC300 presented a Type IV adsorption-desorption isotherm, typical of mesoporous materials, with a hysteresis loop located at 0.4-0.6 relative pressure range, due to capillary condensation within mesopores [88,89]. It is also worth noting that TiO₂-ACAC300 presented lower volumes of gas adsorbed when compared to TiO₂-ACAC and TiO₂-ACAC270, which is an indicative of a lower surface area.

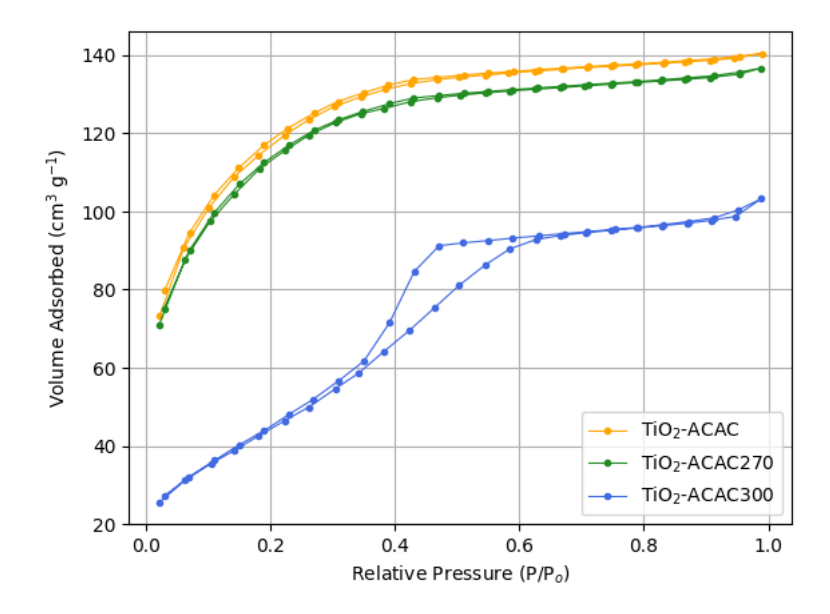


Figure 13: N₂ adsorption-desorption curves for TiO₂-ACAC CTCs

Microporosity of TiO₂-ACAC and TiO₂-ACAC270 can be explained by the presence of ACAC during sol-gel synthesis, which reduces hydrolysis reaction rates and, consequently, promotes smaller particle and pore sizes. However, since TiO₂-ACAC300 was subject to calcination at a slightly higher temperature and for a longer period, an increase particle size takes place, turning it into a mesoporous nanomaterial [16,90]. The effect of calcination is observed in the specific surface area, calculated by BET method, of each photocatalysts, as presented by Table 4. Both TiO₂-ACAC and TiO₂-ACAC270 show rather approximate specific areas of around 400 m² g⁻¹, while TiO₂-ACAC300 suffered a significant decrease in specific surface area.

Table 4: BET Specific area of TiO₂-ACAC nanopowders

Sample	BET Specific Area (m ² g ⁻¹)
TiO ₂ -ACAC	406
TiO ₂ -ACAC270	393
TiO ₂ -ACAC300	171

TGA analyses of TiO₂-ACAC, TiO₂-ACAC270 and TiO₂-ACAC300 samples were performed to determine the overall percentage of ACAC onto titania. TGA curves, presented in Figure 14, evidence three mass loss events of different proportions for each sample. The first event ends at roughly 150 °C and corresponds

to the loss of humidity. The second one, observed between 150 °C and 250 °C, is related to volatilization of weakly bonded ACAC molecules (secondary bonding) and dehydroxilation of surface Ti-OH groups, and a final one from 250 °C to approximately 500 °C, related to thermal degradation of ACAC bonded directly to TiO₂ surface [16]. As anticipated, calcination drastically reduced the overall content of ACAC directly bonded to the surface of TiO₂, from roughly 9.6%, observed in the xerogel, to approximately 4.0% and 2.0% in TiO₂-ACAC270 and TiO₂-ACAC300, respectively. It is important to clarify that calcination was performed not only to improve anatase crystallinity, but also to remove excess ACAC, i.e. weakly bonded ACAC molecules, as it leads to occupation of actives sites at photocatalyst surface and severely hinders the photocatalytic process.

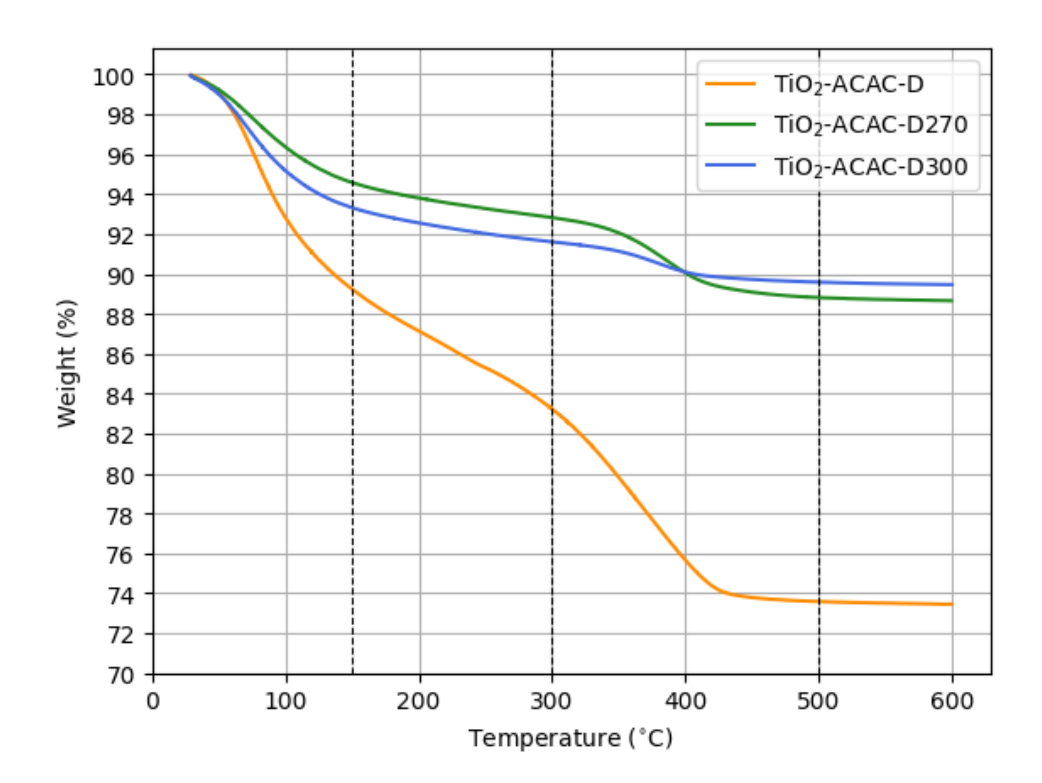


Figure 14: TGA of TiO₂-ACAC CTC nanopowders

To further evidence the coupling of ACAC onto the surface of titania nanoparticles, FT-IR analysis was performed, as shown by Figure 15. All obtained spectra share similar absorption bands, most of which are related to bond vibration within ACAC. The first major band is located at 1620 cm⁻¹ and is attributed to C=C stretching vibrations due to keto-enolic tautomerization of ACAC [91]. The bands located at 1500, and 1415 cm⁻¹ correspond to asymmetric and symmetric stretching, respectively, of the carboxyl group. The narrow band located at 1390 cm⁻¹ and the

broad and weak band at 1370 cm⁻¹ were attributed, respectively, to asymmetric and symmetric bending of the methyl group. Effective coupling of ACAC onto titania can be verified by the almost complete disappearance of the bands located at 1720 and 1760 cm⁻¹, originally attributed to asymmetric and symmetric stretching of C=O in the keto form, since bonding of ACAC to TiO₂ occurs by the carbonyl group. FT-IR spectra also show an absorption band at 1570 cm⁻¹, attributed to O-H symmetrical stretching of water molecules. This band drastically recedes in the FT-IR spectra of calcinated samples, to the point of virtually disappearing in TiO₂-ACAC300, as the material presents little to no residual moisture [16,78].

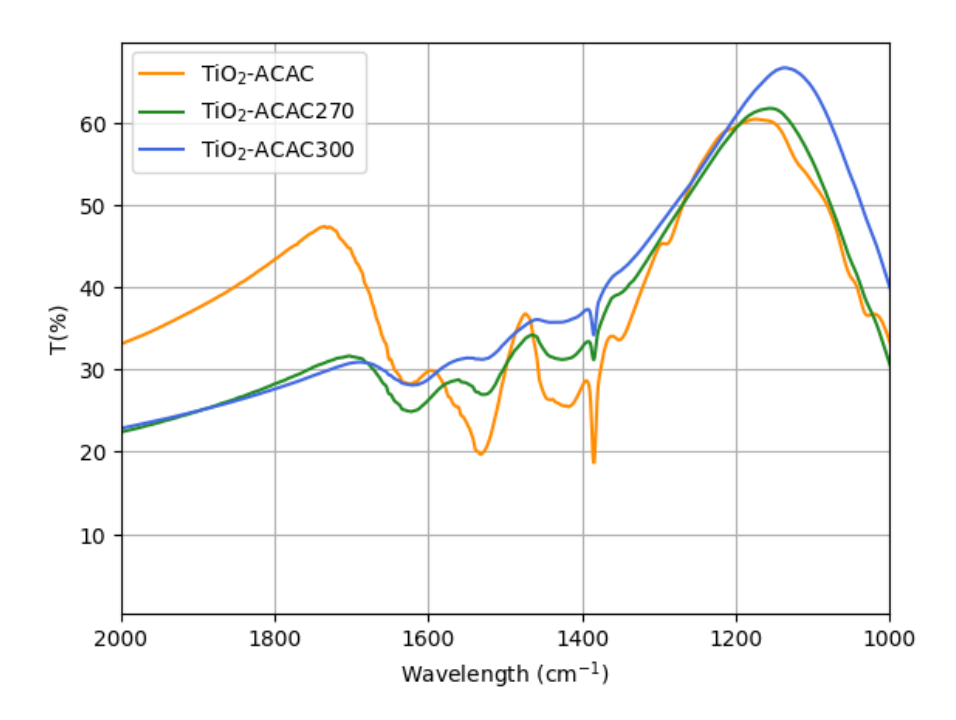


Figure 15: FT-IR spectra of TiO₂-ACAC CTC nanopowders

As it will be further evidenced, each TiO₂-ACAC CTC presented varying photocatalytic activities, which could be due to different single electron trapped oxygen vacancies (SETOV) concentrations, which was determined through EPR analysis. The EPR spectra of TiO₂-ACAC CTCs, depicted in Figure 16, showed paramagnetic signals with varying intensity for each material. TiO₂-ACAC270 presented the highest SETOV, at 7.5×10¹⁶ cm⁻³, while TiO₂-ACAC300 and TiO₂-ACAC exhibited SETOV values of 4.5×10¹⁶ and 6.9×10¹⁶ cm⁻³. Just as reported by Almeida *et al.* (2020), another less prominent feature common to all spectra, is the presence of O-2 signal, observable under visible light [16]. It is worth noting that each EPR curve presents a slight shift relative to one another, since EPR readings

were not performed simultaneously in the presence of a standard sample and g factor was not obtained and, therefore, each measurement was susceptible to variation of microwave frequencies.

The presence of oxygen vacancies in photocatalysts may be both beneficial and detrimental to photocatalytic activity. If present in the bulk, oxygen vacancies may act as undesired recombination centers for charge carriers, while when present on the surface, an increase of active sites and enhancement of charge separation are promoted, effectively favoring the photodegradation process. Therefore, an optimal concentration and distribution of SETOV is desirable in order to maximize active sites and ROS production and minimize charge carrier recombination in bulk oxygen vacancies [78].

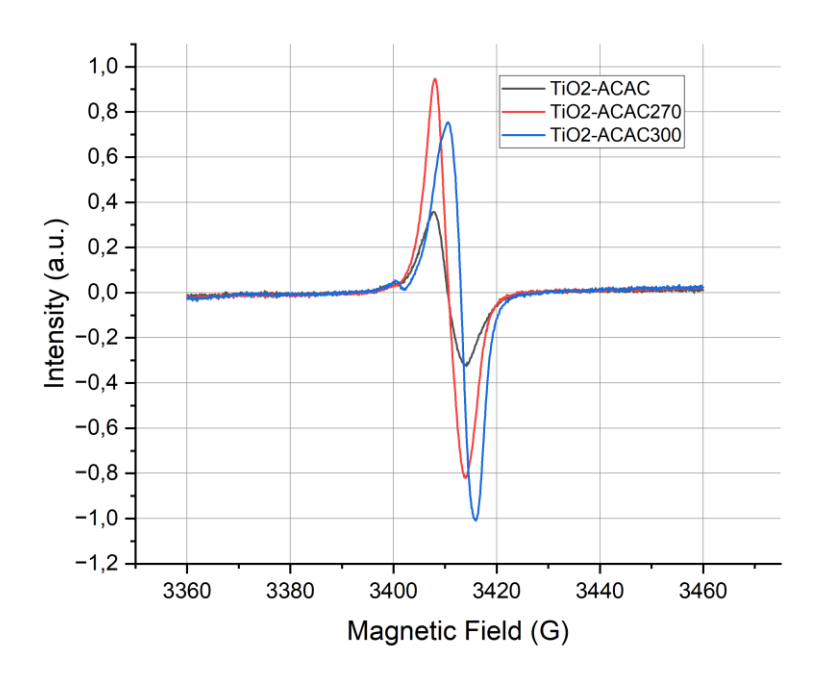


Figure 16: EPR spectra of TiO₂-ACAC CTC nanopowders

Morphological analysis of TiO₂-ACAC CTCs by SEM (Figure 17) shows the formation of agglomerates of varying sizes, from <10 μm to upwards of 50 μm in diameter. In order to investigate the morphology and size of the nanoparticles themselves, TEM analysis was performed and are illustrated in Figure 18. TEM images reveal that the agglomerates are indeed composed of numerous irregular-shaped nanoparticles with less than <10 nm in diameter, in good agreement with the mean crystallite size estimated by XRD. It is also possible to observe the

diffraction of the electron beam by the crystallographic planes of anatase. A similar morphology was reported by Siwinska-Stefanska *et al.* (2015), where the authors also synthesized TiO₂ nanoparticles via sol-gel method and ACAC as chelating agent. In their study, TEM images revealed the presence of irregular shaped clusters formed primarily by nanoparticle agglomerates [92].

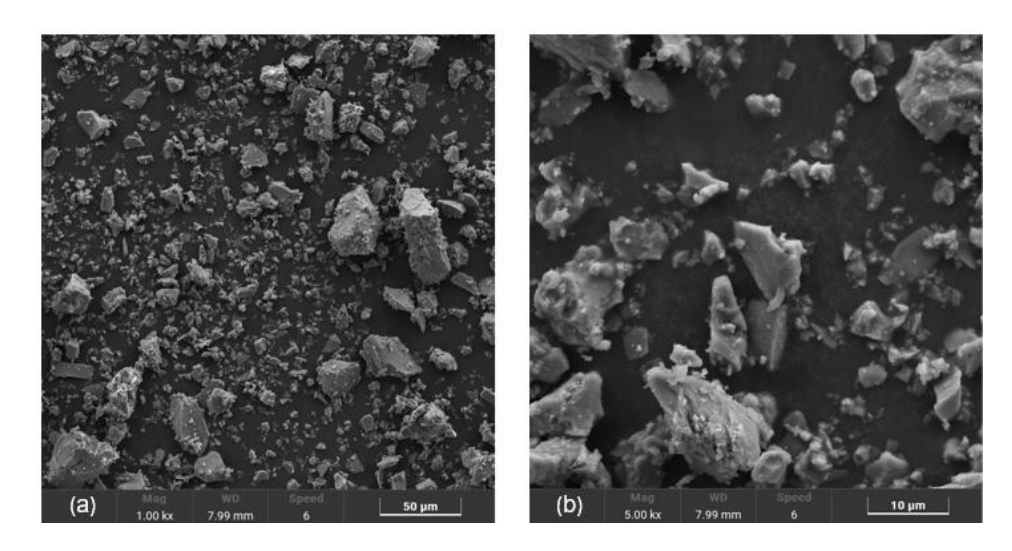


Figure 17: SEM images of TiO₂-ACAC300 nanopowder magnified at 1000x (a) and 5000x (b)

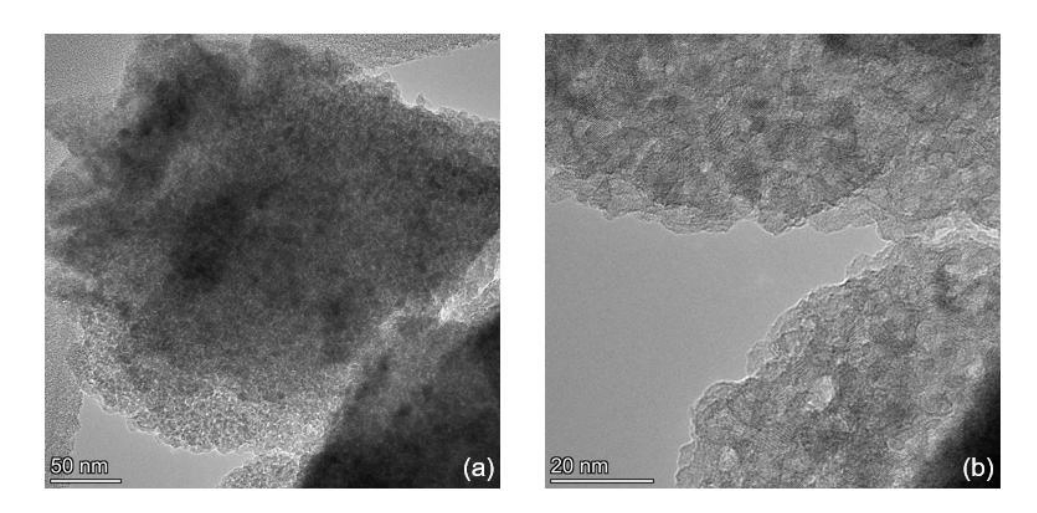


Figure 18: TEM images of TiO₂-ACAC300 nanopowder.

The three TiO₂-ACAC samples were finally submitted to screening photodegradation tests under visible light in the presence of TC as the target pollutant to determine the one with the highest photocatalytic activity, hence elected for the studies with immobilization onto PS matrix. The results, inclusive of a blank experiment without photocatalyst (photolysis), are illustrated in Figure 19.

TiO₂-ACAC xerogel only degraded approximately 45% of TC, during the period of 6 h, presenting the lowest conversion of the prepared CTCs. The low photo-activity of the xerogel is mainly due to two main factors; its low crystallinity, which significantly hinders charge carrier mobility and the excess of ACAC, which may occupy active sites and interfere in ROS formation [16,78]. TiO₂-ACAC270 presented a TC conversion of 53% of TC, a marginal improvement over the xerogel's performance. This result shows a significant decrease in photocatalytic activity if compared to the work of Gil-Londoño et al., where TiO₂-ACAC calcined at 270 °C was capable of degrading roughly 70% of TC in the same amount of time [78]. The reduction of TiO₂-ACAC270 photocatalytic activity may be due to not only the excess of ACAC still present after calcination but also due to the high SETOV concentration, which was more than two orders of magnitude higher than previously reported. Finally, TiO2-ACAC300 was capable of degrading up to 92% of TC and, therefore, was selected as the active phase for the studied PS composites. The photocatalytic performance of TiO₂-ACAC300 surpassed the ones reported by Almeida et al. which could be due to further removal of excess ACAC during calcination and higher surface area [16].

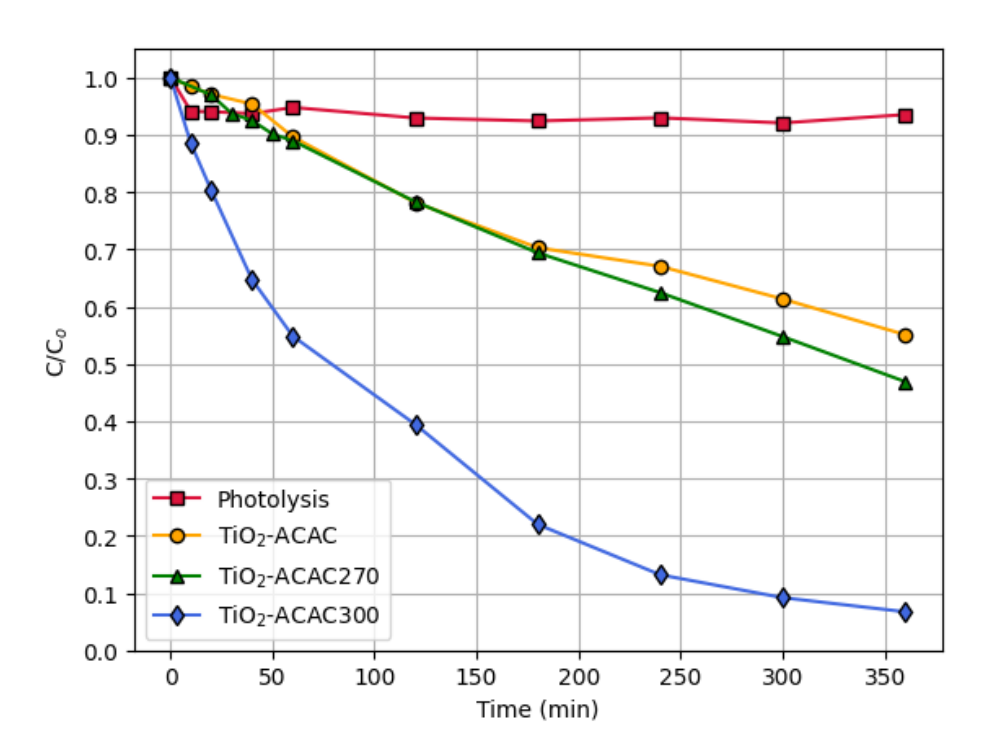


Figure 19: Photocatalytic performance of TiO₂-ACAC CTCs for tetracycline degradation under visible light.

The photodegradation percentage of TC was calculated by the decrease of its absorption peak at 358 nm wavelength. In the cases of TiO₂-ACAC270 and, especially TiO₂-ACAC300, a hypochromic shift of the band centered at 276 nm is observed in UV-Vis spectrum (Figures 20-a and 20-b), which could be an indicative that TC molecule is not being fully mineralized, but rather converted into intermediate species, during photooxidative reactions. To investigate that hypothesis, multiple samples of the reaction media were subjected to TOC analysis, Figure 20-c. TOC results indicate that mineralization occurs only within the first hour of reaction, and is followed by stabilization of TOC in the media, confirming the presence of TC intermediates [93]. It is worth noting that for TiO₂-ACAC270 the hypochromic shift starts to increase after the 120 min mark, which more approximately coincides with TOC stabilization. The same phenomenon is even more perceptible in the case of TiO₂-ACAC300 where a significant hypochromic shift starts at the 120 min mark and coincides precisely with TOC stabilization.

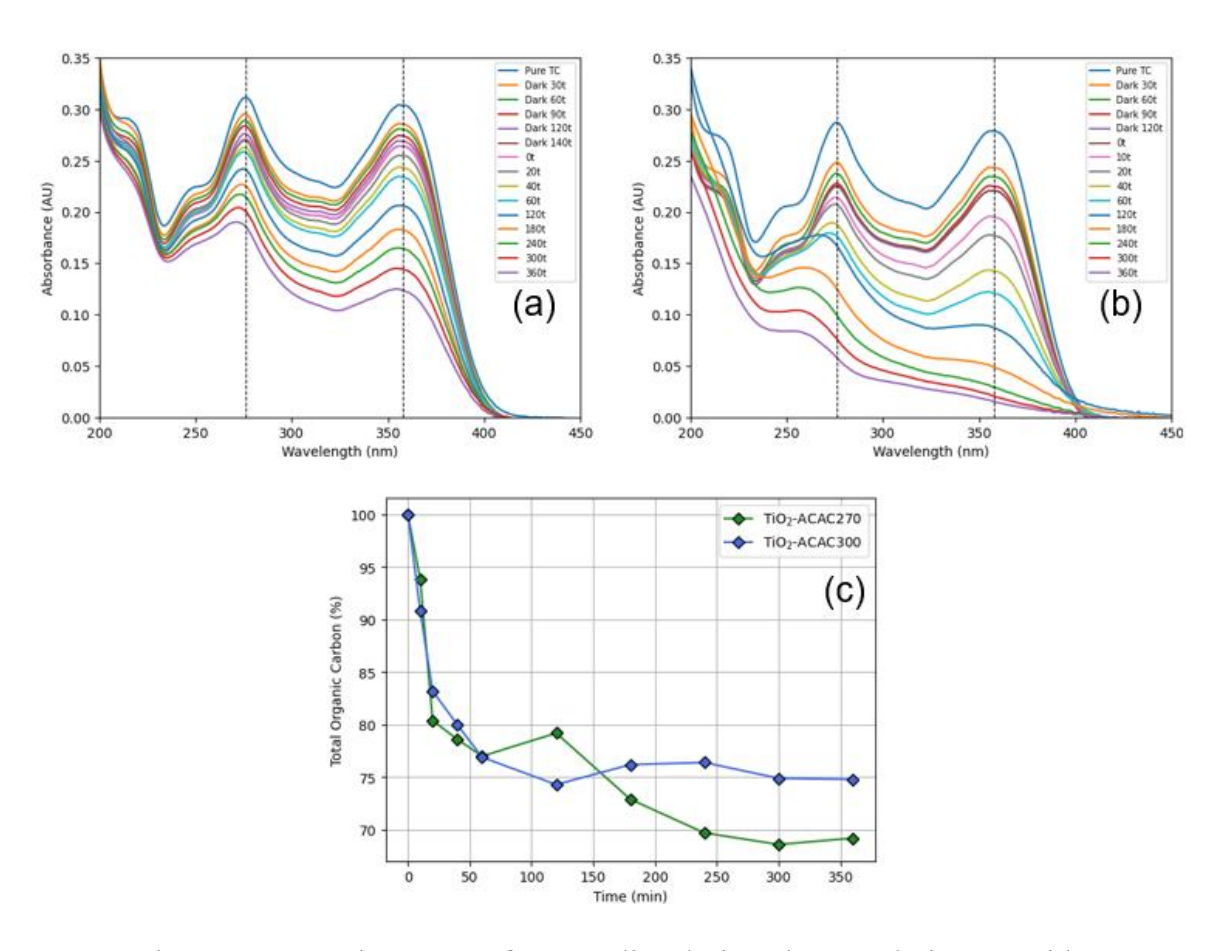


Figure 20: UV-Vis spectra of tetracycline during photocatalytic tests with TiO₂-ACAC270 (b) and TiO₂-ACAC300 (b), TOC presence in reaction media (c)

The incomplete mineralization of pollutants and, more specifically, TC, during photocatalysis have also been previously reported. For instance, Zhu *et al.* reported, in a similar experiment using TiO₂ nanoparticles, degradation of upwards of 95% of TC, but removal of only 40% of TOC in the reaction media [94]. In a more recent study, Patidar *et al.* also reported high photodegradation efficiency of TC using carbon doped titania nanoparticles under UV light, but mineralization only took part during the first 30 min and stabilized at roughly 60% of TOC content [95]. Regarding the possible intermediate species, originating from partial breakdown of TC molecules, numerous photodegradation pathways have been proposed [94,95,96]. However, determining the possible byproducts of TC degradation by TiO₂-ACAC CTCs is not only a relatively complex task, but also is not within the proposed scope of the present work.

4.3.2 Characterization and Photocatalytic Performance of PS-based composites

As previously mentioned, since TiO₂-ACAC300 showed a superior photocatalytic performance, it was chosen as the active phase of the PS composites. To verify if nanoparticle immobilization had fully occurred in accordance with the stipulated 30 and 50% percentages of active phase, TGA were performed, first with both NIPS and TIPS composites, which are shown in Figures 21-a and 21-b, respectively. TGA was also performed on pure (no active phase) NIPS and TIPS foams, to determine the presence of impurities or inorganic additives in PS.

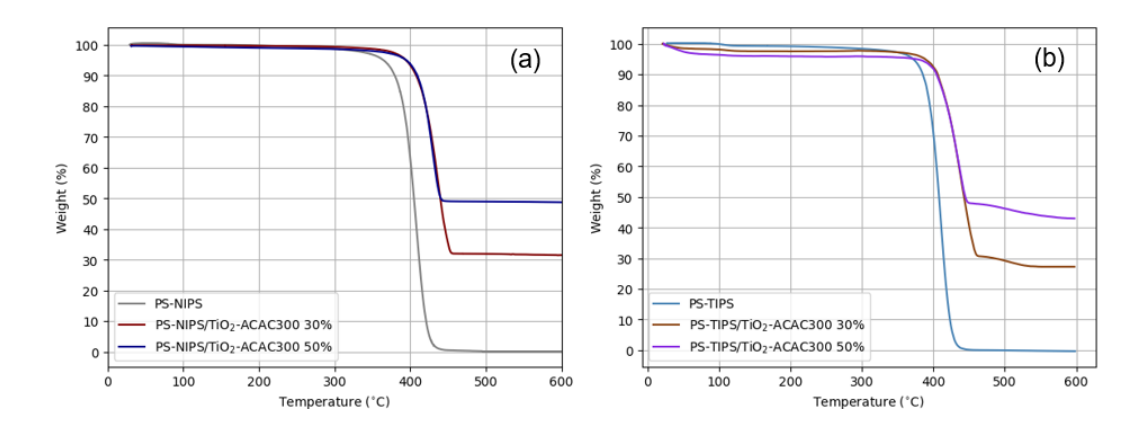


Figure 21: (a) TGA curves of NIPS and; (b) TIPS composites/foams

From Figure 21-a, it can be observed that both PS-NIPS/TiO₂-ACAC composites presented TiO₂ percentages close to the expected values of 30% and 50%, with small variation that might be attributed to some heterogenous dispersion of nanoparticles within the matrix. PS-NIPS TG curve also revealed complete PS degradation just after 400 °C, indicating that no inorganic contaminants or additives were significantly present. On the other hand, Figure 21-b shows that PS-TIPS/TiO₂-ACAC300 (30%) roughly achieved the desired 30% active phase composition, while its TIPS/TiO₂-ACAC300 (50%) presented approximately 42% of titania, indicating a significant loss of active phase during immobilization. It is important to note that the presence of ACAC was not taken into consideration, as it would have a minimal impact on the active phase percentage of the composites.

Nitrogen adsorption-desorption isotherms of NIPS and TIPS samples (pure and composites) are shown in Figure 22-a and 22-b, respectively. Both NIPS and TIPS composites show Type IV isotherms, due to the presence of mesoporous TiO₂-ACAC300 nanoparticles. However, TIPS composites also present a small secondary hysteresis loop, present at < 0.9 relative pressure range, likely related to capillary condensation in the pores of PS matrix.

Both pure PS-NIPS and PS-TIPS samples present the same Type II isotherm, typical of non-porous or, in this case, macroporous materials, with very low total N₂ volume adsorbed due to their low specific area and no significant hysteresis [21,89].

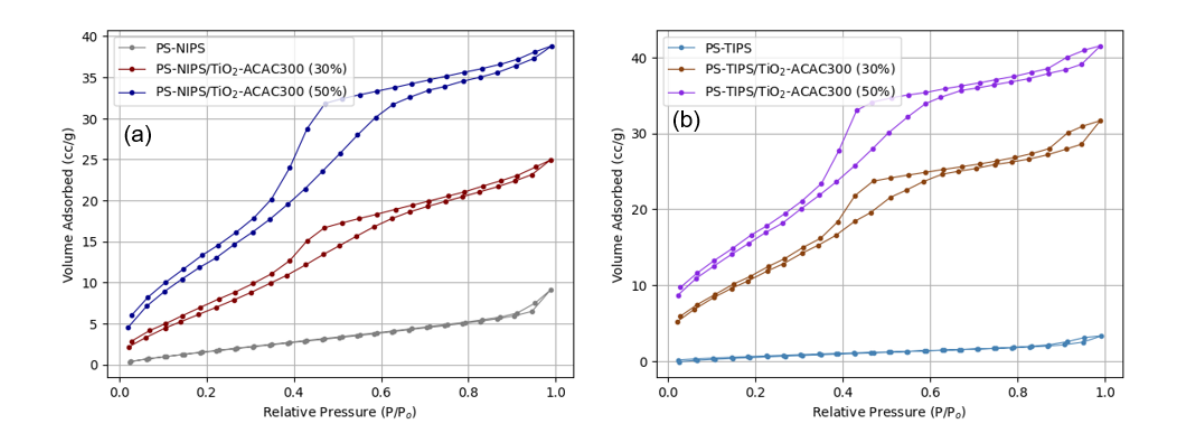


Figure 22: N₂ adsorption-desorption isotherms for NIPS (a) and TIPS (b) samples

The BET specific areas of NIPS and TIPS samples are shown in Table 5. Pure PS-NIPS presented a specific area almost three times larger than the pure PS-TIPS sample; an indicative of a more porous structure and/or with smaller pores. On the other hand, both PS-TIPS composites presented a higher specific area than the corresponding NIPS composites, which is a strong indicative that TIPS composites achieved a more homogenous dispersion of the nanoparticles with less agglomerates and/or less nanoparticle occlusion.

Both NIPS and TIPS composites, however, presented specific areas below the expected values based on the loading percentage of TiO₂-ACAC300 with BET S.A. of 171 m² g⁻¹, as shown in Table 5. This considerable area loss is even more evident if the theoretical S.A. values (Equation 1) are compared to the experimental areas. These results strongly suggest that nanoparticle agglomeration and encapsulation by the PS matrix has occurred and is even more prominent in NIPS composites.

Table 5: Experimental (BET) and Theoretical Specific Area of NIPS and TIPS samples

Sample	BET Specific Area (m² g-¹)	Theoretical Specific Area (m ² g ⁻¹)	Discrepancy*
PS-NIPS	8.62		
PS-TIPS	3.29		
PS-NIPS/TiO ₂ -ACAC300 (30%)	31.4	57.3	-45.2%
PS-TIPS/TiO ₂ -ACAC300 (30%)	45.9	50.2	-8.56%
PS-NIPS/TiO ₂ -ACAC300 (50%)	54.4	89.8	-39.4
PS-TIPS/TiO ₂ -ACAC300 (50%)	63.6	73.7	-13.7

^{*}Discrepancy was calculated as $(\frac{A_{BET}-TSA}{TSA}) \times 100$

Results of density measurements, made by the Archimedes principle are presented in Table 6. In the range of 10-50% of titania content, TIPS composites showed slight increments in density, reaching a maximum of 0.34 g cm⁻³ for 50% of titania loading. Due to their extremely low density, TIPS composites strictly float in water and are unable to disperse to the bulk of an aqueous media, even if agitation

is present, which, as it will be further evidenced, may compromise its photocatalytic performance. NIPS composites on the other hand, showed a significant increase in density with progressive photocatalyst loading. With only 30% of titania loading, NIPS composites presented, on average, a density of 0.61 g cm⁻³, which allow the beads to both float and disperse into the bulk of the solution when agitation is present, effectively enhancing reaction media coverage. It is worth noting that density measurements of NIPS composites were not performed for higher percentages of photocatalyst loading due to an excess of particle detachment, which led to imprecise readings.

Table 6: Density measurements of NIPS and TIPS composites

Titania Percentage	Density of NIPS composites (g cm ⁻³)	Density of TIPS composites (g cm ⁻³)
10%	0.17	0.24
20%	0.19	0.50
30%	0.23	0.61
40%	0.27	
50%	0.34	

Surface SEM images of pure PS-NIPS, shown in Figures 23-a and 23-b, reveal relatively smooth surface of PS beads, with a few irregularities and cavities that reveal a porous structure underneath, containing pores with less than 5 μm in diameter. On the other hand, PS-NIPS/TiO₂-ACAC300 composite's surface presents several photocatalyst agglomerates embedded into the PS matrix (circled in Figure 23-c), which are also present in the cross section of NIPS composites, along with a heterogeneous distribution of macropores (figure 23-d).

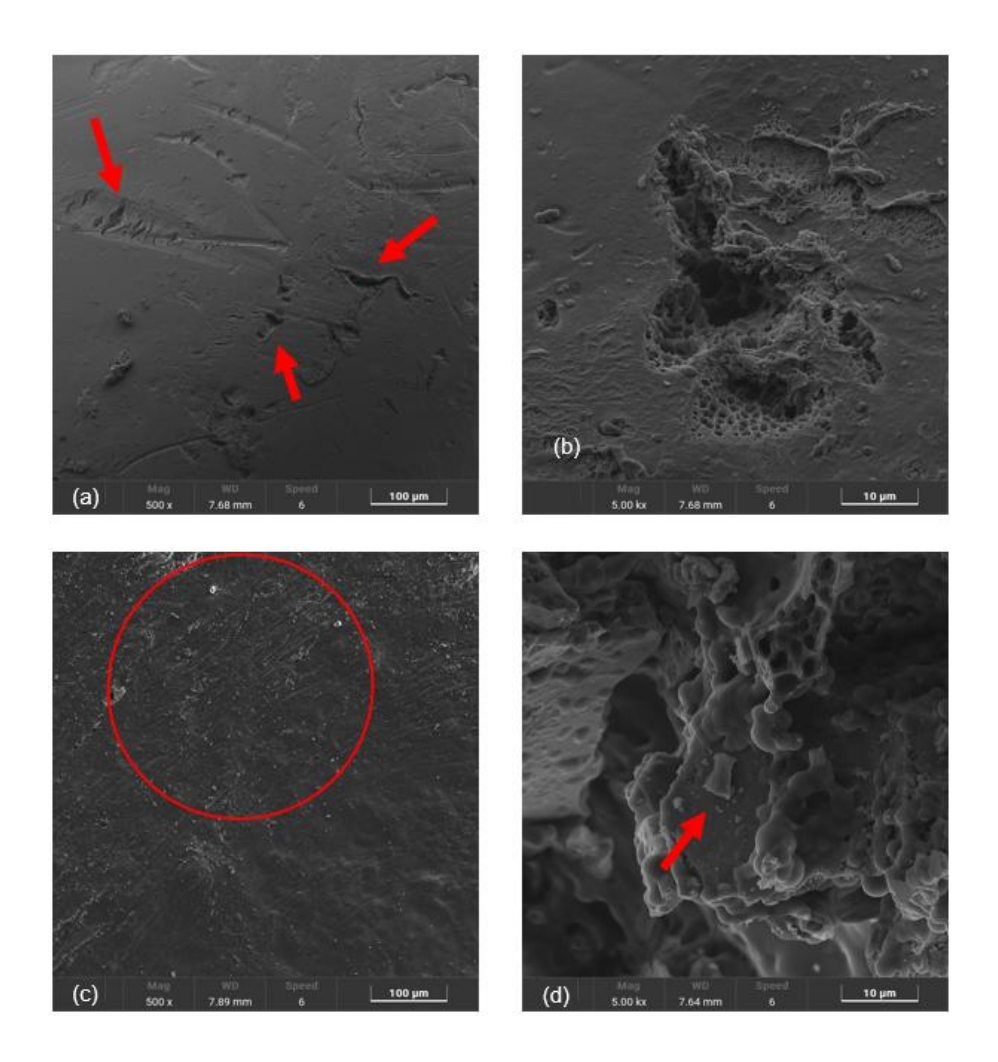


Figure 23: SEM images of pure PS-NIPS foam's surface (a, b) and PS-NIPS/TiO₂-ACAC300 (30%) composite's surface (c) and cross-section (d)

SEM images of pure PS-TIPS foams surface and cross section are depicted in Figures 24-a and 24-b, respectively, which reveal a more homogenous distribution of interconnected macropores (larger than those found in PS-NIPS), both on the materials surface and its interior. TIPS methodology resulted in larger pores, when compared to NIPS route, with pores reaching almost 50 µm in diameter. Figure 24-c shows the surface of PS-TIPS/TiO₂-ACAC300, which also contains macropores along with photocatalyst agglomerates embedded in the PS matrix. However, cross section images of PS-TIPS/TiO₂-ACAC300 composites (Figure 24-d) showed little to no presence of photocatalyst agglomerates or nanoparticles, indicating that their presence was mostly restricted to the material's surface.

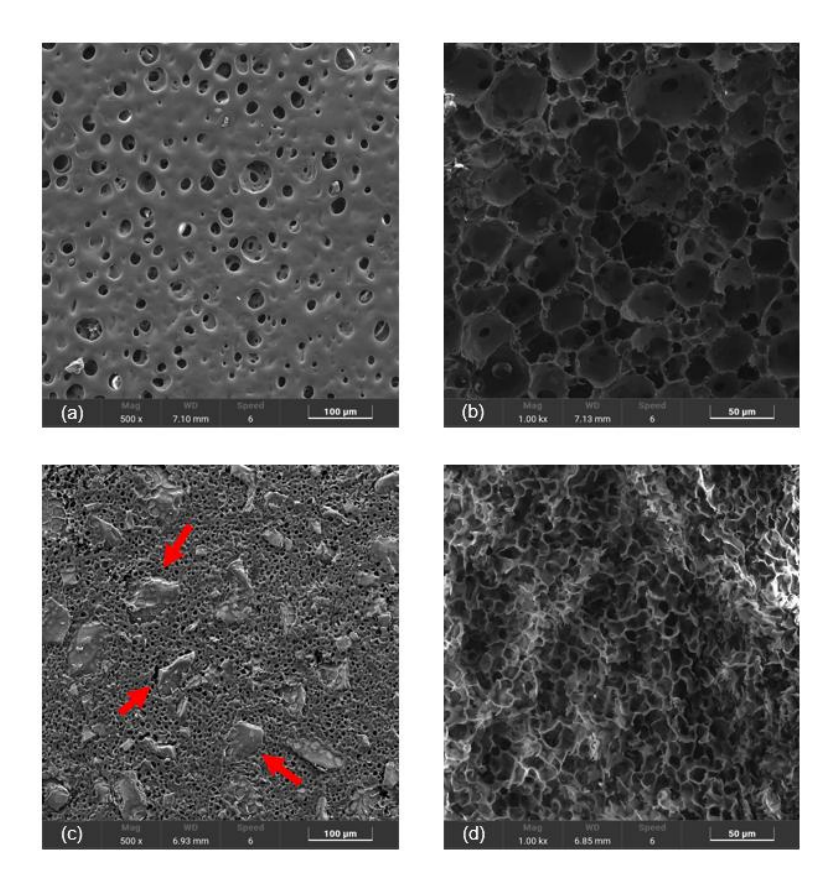


Figure 24: SEM images of pure PS-TIPS foam's surface (a) and cross-section (b), along with PS-TIPS/TiO₂-ACAC300 (30%) composite's surface (c) and cross-section (d)

Regarding the synthesized PS-based floating photocatalysts, NIPS composites were the first to be tested for TC photodegradation. When inserted in aqueous media, both 30% and 50% NIPS composites showed floating capabilities and were able to disperse into the bulk of the solution with agitation. Figure 25 shows the results of TC photodegradation of NIPS composites, as well as of the pure TiO₂-ACAC300 and of the pure TC solution (photolysis) under 100 W visible light irradiation.

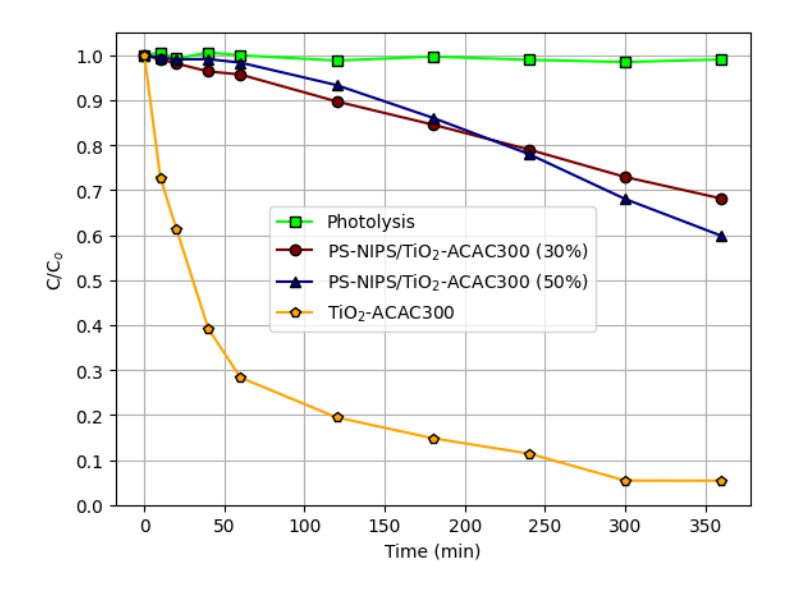


Figure 25: Photolysis and photocatalytic performance of PS/TiO₂-ACAC300 NIPS composites and pure TiO₂-ACAC300 under visible light (100 W) for TC degradation.

As shown in Figure 25, photolysis of TC under 100 W visible light was virtually null while its photocatalytic degradation in the presence of TiO₂-ACAC300 nanopowder reached 95%, comparable to the result obtained under 26 W irradiation (Figure 19). The NIPS composites, however, comparatively presented inferior photocatalytic activity; PS-NIPS/TiO2-ACAC300 (30%) was capable of removing roughly 32% of TC, while PS-NIPS/TiO₂-ACAC300 (50%) showed a marginal improvement and degraded approximately 40% of the contaminant. These findings are in opposition to the predominantly presented in the literature since most reports on floating photocatalysis report either approximate or enhanced photocatalytic performance of floating photocatalysts over their powdered counterparts [18,62,64,68,97]. A few studies, however, have also presented inferior photocatalytic performance of polymer-based floating photocatalysts. For instance, Rosa et al. reported significantly slower photodegradation kinetics of methylene blue in the presence of TiO₂ supported onto PS pellets [84]. In addition, Guo et al., also observed that, when stirring is applied in the reaction media, floating photocatalysts may be less efficient than their powdered counterparts [66].

From Tables 1 and 2, it can also be observed that most studies regarding polymer-based floating photocatalysts carried out photocatalytic tests under more favorable conditions for photocatalysis, such as reduced volume (< 100 mL), high

photocatalyst concentration and high-power light sources. However, it still would not completely explain the drastic reduction of photocatalytic activity presented by the composites, especially since both TGA and SEM revealed successful nanoparticle immobilization both onto PS beads surface and into its porous structure.

A formulated hypothesis for the reduced photocatalytic activity of NIPS composites is a possible deactivation of the CTC effect of TiO₂-ACAC while manufacturing the PS-NIPS composite. To test this hypothesis, new PS-NIPS composites were prepared using TiO₂-P25 as the active phase, since it's a well-known photocatalysts, with numerous reports of its high photodegradation capabilities in aqueous media [98]. The synthesis of PS-NIPS/P25 composites followed the exact same procedure of PS-NIPS/TiO₂-ACAC300 materials. Their TG and BET adsorption-desorption curves are represented in Figures A1 and A2, respectively, while BET Surface Areas are listed in Table A1. The photocatalytic experiments were conducted, just as previously described for PS-NIPS/TiO₂-ACAC300 composites, except for the usage of a 36 W UV lamp as the light source. TC photolysis and photodegradation using pure P25 were also performed, and the results are shown by Figure 26.

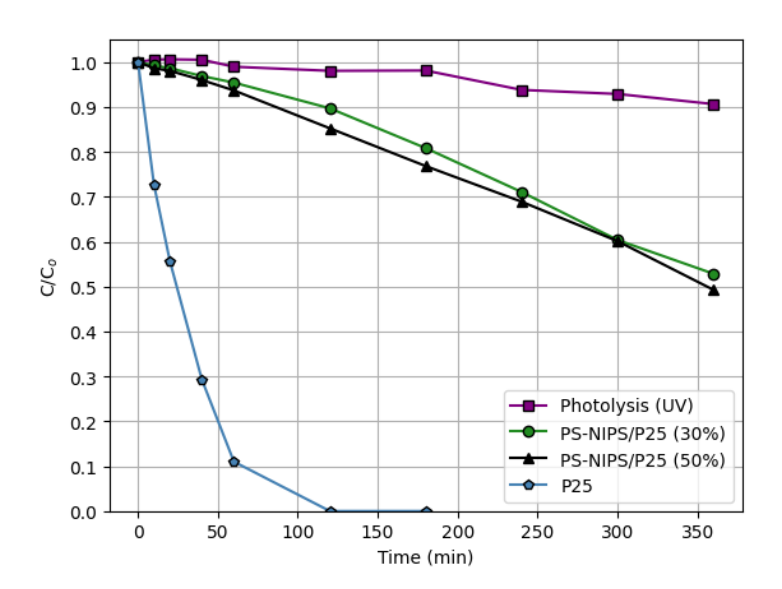


Figure 26: Photolysis and photocatalytic performance of PS/P25 NIPS composites and pure P25 under UV light.

TC photolysis under UV light reached approximately 10% after 6 h, while pure P25 was capable of totally photodegrading TC after 3 h. However, both PS-

NIPS/P25 composites, containing 30% and 50% of photocatalyst loading, also presented a drastic reduction in photocatalytic activity, just as observed for PS-NIPS/TiO₂-ACAC300 composites. PS-NIPS/P25 (30%) degraded TC by about 47%, while PS-NIPS/P25 (50%) showed a minute improvement on photocatalytic performance and degraded around 51% of the contaminant after 6 h. These results rule out the aforementioned hypothesis of TiO₂-ACAC inactivation during solvent-aided preparation of the composite and, thus, further investigation was required.

A second hypothesis that might explain the diminished photocatalytic performance of the as synthesized PS-based floating photocatalysts, is the NIPS immobilization technique itself, which, according to Tables 5 and A1, led to a more prominent nanoparticle occlusion and may lack of homogenous porous structure, compromising photocatalytic activity.

This conjecture was put to the test with PS-TIPS/TiO₂-ACAC300 composites, which not only did the SEM images reveal to the presence of homogenous distribution of macropores and presence of photocatalyst poder on its surface but also BET surface areas were superior to those of PS-NIPS/TiO₂-ACAC300, indicating that TIPS methodology led to less nanoparticle encapsulation. As previously discussed, TIPS composites were prepared mostly in accordance with De Assis *et al.*, whose work reports highly active PS@SnO₂ photocatalytic foams under UV-light [18].

For the sake of direct comparison, photocatalytic experiments were conducted the same way as NIPS composites. Unfortunately, however, as evidenced by Figure A3, PS-TIPS/TiO₂-ACAC300 composites performed even worse than their NIPS counterparts, yielding virtually zero photocatalytic activity, hence these experiments were cut short after 3 h. The results obtained for TIPS composites do not corroborate the findings of De Assis *et al.* but could be partially explained by different reactor configuration and the fact that, unlike NIPS beads, TIPS composites strictly float, even in the presence of agitation, which severely limits reaction media coverage.

One third, and final, hypothesis for reduced photocatalytic performance of the floating composites is the partial degradation of PS matrix either due to agitation (physical) or photo-induced reactions (chemical). If the PS matrix is truly being degraded during photocatalytic process, microplastics and/or PS-byproducts would be released into the reaction media, both promoting light scattering and competition for active sites with TC. This hypothesis has been raised after the works of various authors, who reported photocatalysis to be an efficient method of PS degradation [73,74,75,98].

4.3.3 Evaluation of Physical and Photochemical Stability of PS Matrix

To verify signs of degradation of the PS matrix, the NIPS composites, after photocatalytic tests, were analyzed by SEM (Figure 27). The surface of used NIPS beads presented roughness and irregularities that were otherwise absent before their use in photocatalytic tests (Figure 23). Moreover, a few cavities were also present on the surface but are not necessarily related to PS degradation and could be attributed to detachment of agglomerates. However, the cross-section of NIPS composites, shown by Figures 27-c and 27-d, evidence clear signs of photochemical degradation, as multiple circle-shaped craters are present. Considering SEM images of NIPS composites before their use in photocatalytic tests (Figure 23), it seems that these cavities are not pores, as they are much larger and prominent; most reaching upwards of 50 µm. Similar observations were also made by Shang *et al.*, who also reported an increase in quantity of cavities and their diameters, after fluorescent light exposure in the presence of TiO₂ particles [75].

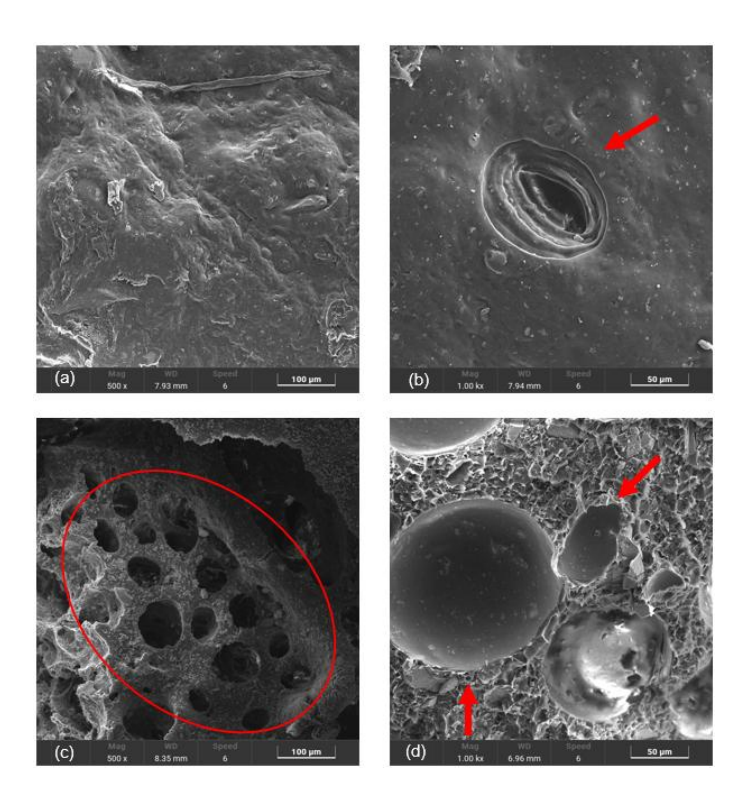


Figure 27: SEM images of PS-NIPS/TiO₂-ACAC300 (30%) surface (a, b) and cross-section (c, d) after photocatalytic tests

Since SEM images of used PS-NIPS/TiO₂-ACAC300 composites showed signs of PS degradation, non-used NIPS floating photocatalysts were used in TOC analysis, as similarly performed by García Muñoz *et al.* [74]. As previously mentioned for the first three experiments, the system was kept in the dark, under agitation, while the second set of experiments were performed with light irradiation. Figure 28 shows TOC results from the samples taken from the two sets of tests.

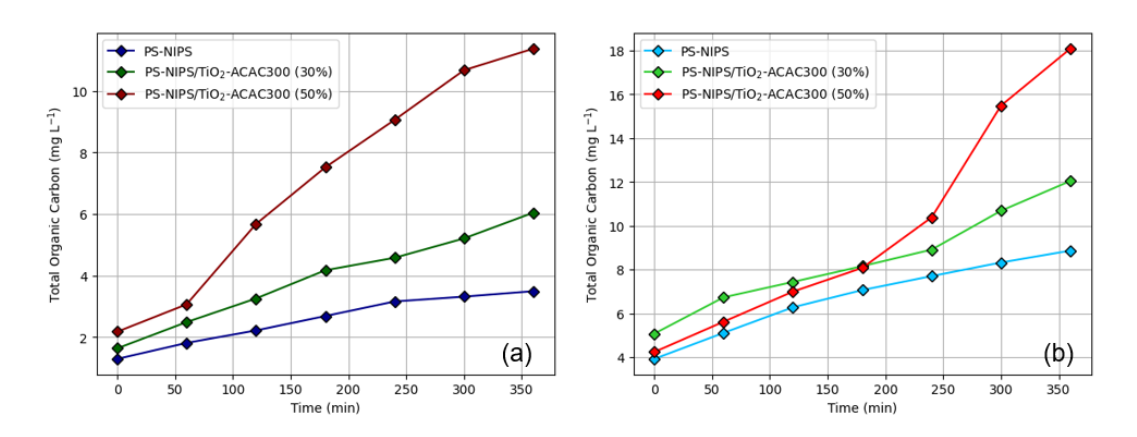


Figure 28: TOC analysis of NIPS samples in the dark, under agitation (a) and under 100 W visible light irradiation and agitation (b).

As seen in Figure 28-a, all NIPS samples in aqueous media, under agitation, in the absence of light irradiation produced organic content in the reaction environment.

PS-NIPS and PS-NIPS/TiO₂-ACAC300 (30%) show a steady and approximately linear increase of TOC over time (6 h), while PS-NIPS/TiO₂-ACAC300 (50%) present and an abrupt rise in organic content release rate after the 1 h of agitation in dark. The results for the initial TOC set of experiments in the dark show that PS based composites are prone to generating secondary pollution, *i.e.* microplastics, when subjected to agitation in aqueous media, which severely compromises their usage for wastewater treatment.

In addition, the results of TOC analysis of NIPS samples subjected to 100 W visible light irradiation cast doubt over PS photochemical stability during photolysis and photocatalytic process. TOC results of NIPS samples irradiated with visible light are shown in Figure-28b, which not only also evidence a significant increase of TOC for the same three samples, but also the overall carbon content was even higher than the set of tests in the dark (Figure 28-a). This second set of results strongly suggests that the presence of a light source may promote photodegradation of PS matrix, which is in line with the deterioration detected by SEM analysis on used PS-NIPS/TiO₂-ACAC300 composites, thus confirming the potential of secondary pollution by microplastics and/or PS degradation byproducts.

In light of the results presented, multiple factors can be cited to explain the lower photocatalytic activity of PS-based floating photocatalyst in the degradation of TC: (i) Nanoparticle occlusion by PS matrix, effectively lowering the number available active sites and promoting poor light harvesting, (ii) poor coverage of the reaction media by the floating photocatalysts, especially in relatively high volume of water, (iii) release of secondary pollution by PS matrix, which not only contributes to solution murkiness and light scattering, while also may compete for photocatalyst active sites along with TC. Although synthesized PS-based photocatalytic composites are easier to recover from the reaction media, their poor photocatalytic performance due to the listed factors severely compromises real world applications and, therefore, were not used in multiple cycles of photocatalytic tests.

5 Conclusions and proposals for future research

TiO₂-ACAC CTC nanopowders were successfully synthesized by sol-gel method and applied in preliminary photodegradation tests in the presence of tetracycline (TC). TiO₂-ACAC300 nanopowders, calcined at 300 °C for 3 h, showed the best photocatalytic performance, under visible light, reaching upwards of 92% of TC photodegradation after 6 h. Despite its appreciable photodegradation capabilities, TOC content indicated relatively constant value of 25% of TC mineralization after 120 min, demonstrating that photo-oxidation of TC have preferably led to intermediate products.

Due to its high photocatalytic performance, TiO₂-ACAC300 nanopowders were immobilized onto PS matrix by NIPS and TIPS methods, forming floating photocatalytic composites, containing 30% and 50% of active phase. TGA shows that the desired active phase percentages were mostly achieved. However, the composites showed a significant specific area reduction per content of photocatalyst, when compared to non-immobilized TiO₂-ACAC300. SEM images revealed that NIPS composites had TiO₂-ACAC300 agglomerates adhered both on the surface and the interior of the beads, with a heterogeneous porous structure. TIPS composites, on the other hand, presented TiO₂-ACAC300 agglomerates mostly adhered to its surface and a more homogenous porous structure.

Photocatalytic tests of NIPS composites revealed a severe reduction of photoactivity in comparison with the corresponding non-immobilized TiO₂ nanopowders. Under visible light, PS-NIPS/TiO₂-ACAC300 composites were capable of degrading only 32-40% of TC after 6 h, compared to over 90% achieved by the TiO₂-ACAC300. Similarly, under UV light, PS-NIPS/P25 degraded only 47-51% of TC whereas full photodegradation has been achieved with pure TiO₂-P25 nanopowder. Such behavior could be directly correlated with the loss of surface area per content of photocatalyst in the composites, thus strongly suggesting that polymer immobilization resulted in TiO₂ particles occlusion.

In contrast, TIPS composites showed virtually no TC degradation. In this case, besides occlusion of TiO₂ particles, most of the lack of photocatalytic activity is probably explained by the much lower density of TIPS composites, leading to poorer reaction media coverage in a high volume of liquid (500 mL) when compared to NIPS composites, which mostly remained submerse in the stirred photoreactor.

SEM images of used NIPS composites (after photocatalytic experiments) revealed some kind of PS matrix deterioration, as deduced by the presence of enlarged cavities and irregularities, suggesting its possible photo-oxidation. TOC analyses using pure PS-NIPS, as well as NIPS composites, in the absence of any other pollutants revealed gradual and significant rise of organic carbon content into the solution, suggesting the release of microplastics from the polymeric matrix, likely promoted by agitation. Additionally, TOC evaluation with visible light irradiation revealed an even higher organic carbon content, which strongly suggests both physical and photochemical degradation of the PS matrix. Consequently, the presence of microplastics and/or PS degradation byproducts not only can worsen solution turbidity and promote light scattering but also may compete with TC for TiO₂ active sites, which help explain inferior photocatalytic performance of the composites.

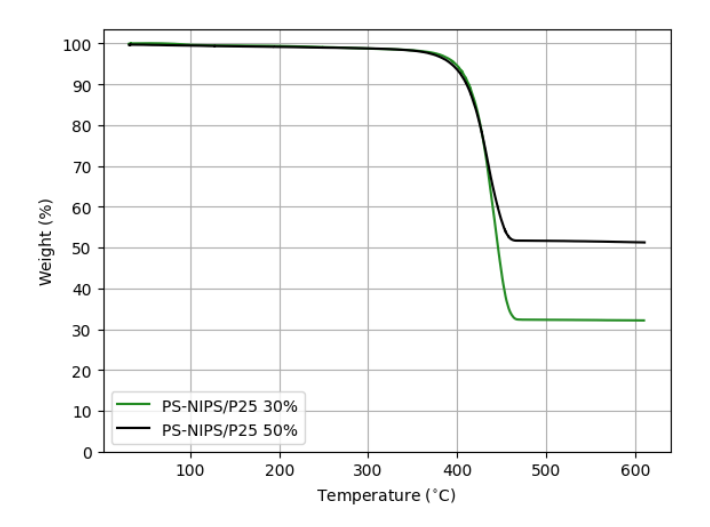
In future works, the authors would like to better investigate the assumed formation of microplastics and/or intermediates with recycled PS based materials. Furthermore, other support materials and immobilization techniques may be tested for preparation of new and more effective floating photocatalysts.

Appendix

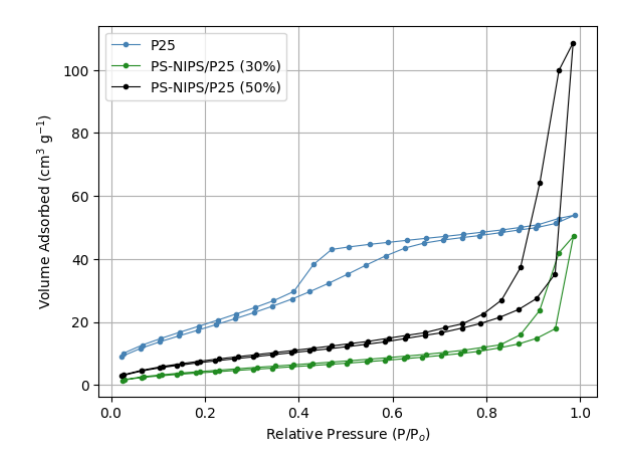
5.1 Supplementary information of chapter 4

A1

TG curves of PS-NIPS/P25 composites



A2
Adsorption-desorption isotherms for TiO₂-P25 and PS-NIPS/P25 composites



A3

UV-Vis spectra of tetracycline in photodegradation experiments using PS-TIPS/TiO₂-ACAC300 (30%) (a) and PS-TIPS/TiO₂-ACAC300 (50%) (b)

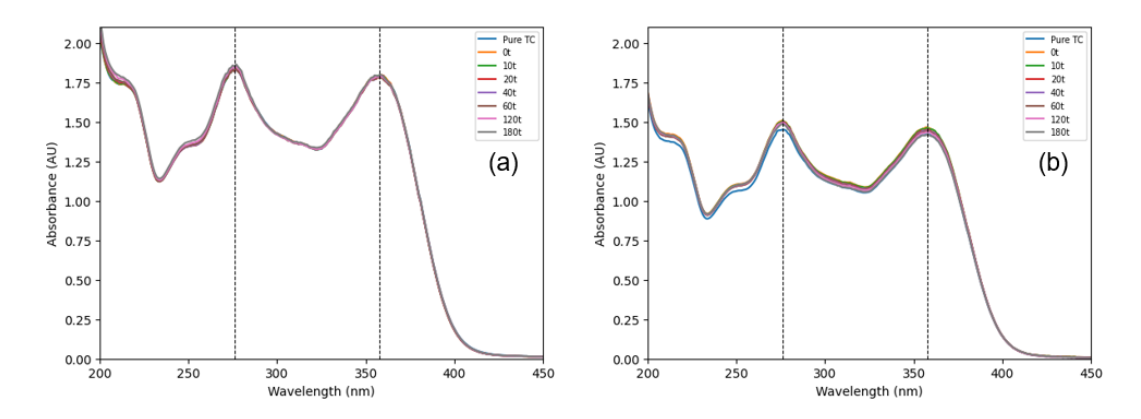


Table A1BET specific area of TiO₂-P25 and PS-NIPS/P25 composites

Sample	BET Specific Area (m² g-¹)	Theoretical Specific Area (m² g-1)	Discrepancy
TiO ₂ -P25	74.6		
PS-NIPS/P25 (30%)	16.8	28.4	-40.8%
PS-NIPS/P25 (50%)	30.2	41.6	-27.4%

References

- [1] RASHID, R. et al. Advancements in TiO2-based photocatalysis for environmental remediation: Strategies for enhancing visible-light-driven activity. **Chemosphere**, v. 349, p. 140703, fev. 2024.
- [2] GUARALDO, T. T. et al. Highly efficient ZnO photocatalytic foam reactors for micropollutant degradation. **Chemical Engineering Journal**, v. 455, p. 140784, jan. 2023.
- [3] LONG, S. et al. Bioadsorption, bioaccumulation and biodegradation of antibiotics by algae and their association with algal physiological state and antibiotic physicochemical properties. **Journal of Hazardous Materials**, v. 468, p. 133787, abr. 2024.
- [4] ZENKER, A. et al. Bioaccumulation and biomagnification potential of pharmaceuticals with a focus to the aquatic environment. **Journal of Environmental Management**, v. 133, p. 378–387, jan. 2014.
- [5] SANTHAPPAN, J. S. et al. Origin, types, and contribution of emerging pollutants to environmental degradation and their remediation by physical and chemical techniques. **Environmental Research**, v. 257, p. 119369, set. 2024.
- [6] AMANGELSIN, Y. et al. The Impact of Tetracycline Pollution on the Aquatic Environment and Removal Strategies. **Antibiotics**, v. 12, n. 3, p. 440, 23 fev. 2023.
- [7] MIRZAHEDAYAT, B. et al. Advances in photocatalytic degradation of tetracycline using graphene-based composites in water: a systematic review and future directions. **Environmental Science and Pollution Research**, v. 31, n. 54, p. 62510–62529, 25 out. 2024.
- [8] VARSHA, M.; SENTHIL KUMAR, P.; SENTHIL RATHI, B. A review on recent trends in the removal of emerging contaminants from aquatic environment using low-cost adsorbents. **Chemosphere**, v. 287, p. 132270, jan. 2022.
- [9] RADWAN, E. K. et al. Recent trends in treatment technologies of emerging contaminants. **Environmental Quality Management**, v. 32, n. 3, p. 7–25, mar. 2023.
- [10] JIANG, J.-Q. The role of coagulation in water treatment. **Current Opinion** in Chemical Engineering, v. 8, p. 36–44, maio 2015.

- [11] BABU PONNUSAMI, A. et al. Advanced oxidation process (AOP) combined biological process for wastewater treatment: A review on advancements, feasibility and practicability of combined techniques. **Environmental Research**, v. 237, p. 116944, nov. 2023.
- [12] KUMARI, P.; KUMAR, A. ADVANCED OXIDATION PROCESS: A remediation technique for organic and non-biodegradable pollutant. **Results in Surfaces and Interfaces**, v. 11, p. 100122, maio 2023.
- [13] ZIA, J.; RIAZ, U. Photocatalytic degradation of water pollutants using conducting polymer-based nanohybrids: A review on recent trends and future prospects. **Journal of Molecular Liquids**, v. 340, p. 117162, out. 2021.
- [14] YASMINA, M. et al. Treatment Heterogeneous Photocatalysis; Factors Influencing the Photocatalytic Degradation by TiO2. **Energy Procedia**, v. 50, p. 559–566, 2014.
- [15] SINGH, S.; MAHALINGAM, H.; SINGH, P. K. Polymer-supported titanium dioxide photocatalysts for environmental remediation: A review. **Applied Catalysis A: General**, v. 462–463, p. 178–195, jul. 2013.
- [16] ALMEIDA, L. A. et al. The Influence of Calcination Temperature on Photocatalytic Activity of TiO2-Acetylacetone Charge Transfer Complex towards Degradation of NOx under Visible Light. **Catalysts**, v. 10, n. 12, p. 1463, 14 dez. 2020.
- [17] LINSEBIGLER, L.; LU, G.; YATES, J. T. Photocatalysis on TiOn Surfaces: Principles, Mechanisms, and Selected Results. [s.d.].
- [18] DE ASSIS, G. C. et al. Conversion of "Waste Plastic" into Photocatalytic Nanofoams for Environmental Remediation. **ACS Applied Materials & Interfaces**, v. 10, n. 9, p. 8077–8085, 7 mar. 2018.
- [19] SAHOO, L. et al. 3D Porous Polymeric-Foam-Supported Pd Nanocrystal as a Highly Efficient and Recyclable Catalyst for Organic Transformations. **ACS Applied Materials & Interfaces**, v. 13, n. 8, p. 10120–10130, 3 mar. 2021.
- [20] DE SOUSA CUNHA, R. et al. A comprehensive investigation of waste expanded polystyrene recycling by dissolution technique combined with nanoprecipitation. **Environmental Nanotechnology, Monitoring & Management**, v. 16, p. 100470, dez. 2021.
- [21] GOLD, V. (ED.). The IUPAC Compendium of Chemical Terminology: The Gold Book. 4. ed. Research Triangle Park, NC: International Union of Pure and Applied Chemistry (IUPAC), 2019.
- [22] MUKHTAR, A. et al. Current status and challenges in the heterogeneous catalysis for biodiesel production. **Renewable and Sustainable Energy Reviews**, v. 157, p. 112012, abr. 2022.

- [23] YANG, X.; WANG, D. Photocatalysis: From Fundamental Principles to Materials and Applications. **ACS Applied Energy Materials**, v. 1, n. 12, p. 6657–6693, 24 dez. 2018.
- [24] ZHU, S.; WANG, D. Photocatalysis: Basic Principles, Diverse Forms of Implementations and Emerging Scientific Opportunities. Advanced Energy Materials, v. 7, n. 23, p. 1700841, dez. 2017.
- [25] CARTER, C. B.; NORTON, M. G. Ceramic Materials: Science and Engineering. New York, NY: Springer New York, 2013.
- [26] SCHNEIDER, J. et al. Understanding TiO₂ Photocatalysis: Mechanisms and Materials. **Chemical Reviews**, v. 114, n. 19, p. 9919–9986, 8 out. 2014.
- [27] GUO, Q. et al. Fundamentals of TiO₂ Photocatalysis: Concepts, Mechanisms, and Challenges. **Advanced Materials**, v. 31, n. 50, p. 1901997, dez. 2019.
- [28] HASSAAN, M. A. et al. Principles of Photocatalysts and Their Different Applications: A Review. **Topics in Current Chemistry**, v. 381, n. 6, p. 31, dez. 2023.
- [29] CHAKRAVORTY, A.; ROY, S. A review of photocatalysis, basic principles, processes, and materials. Sustainable Chemistry for the Environment, v. 8, p. 100155, dez. 2024.
- [30] WANG, H. et al. A review on heterogeneous photocatalysis for environmental remediation: From semiconductors to modification strategies. **Chinese Journal of Catalysis**, v. 43, n. 2, p. 178–214, fev. 2022.
- [31] IBHADON, A.; FITZPATRICK, P. Heterogeneous Photocatalysis: Recent Advances and Applications. **Catalysts**, v. 3, n. 1, p. 189–218, 1 mar. 2013.
- [32] BUNEA, R.; SAIKUMAR, A. K.; SUNDARAM, K. A Comparison of Optical Properties of CuO and Cu<sub>2</sub>O Thin Films for Solar Cell Applications. **Materials Sciences and Applications**, v. 12, n. 07, p. 315–329, 2021.
- [33] JANCZAREK, M.; KOWALSKA, E. On the Origin of Enhanced Photocatalytic Activity of Copper-Modified Titania in the Oxidative Reaction Systems. **Catalysts**, v. 7, n. 11, p. 317, 27 out. 2017.
- [34] LEE, K. et al. Enhancement of TOC removal efficiency of sulfamethoxazole using catalysts in the radiation treatment: Effects of band structure and electrical properties of radiocatalysts. **Separation and Purification Technology**, v. 312, p. 123390, maio 2023.
- [35] KUDO, A.; MISEKI, Y. Heterogeneous photocatalyst materials for water splitting. **Chem. Soc. Rev.**, v. 38, n. 1, p. 253–278, 2009.

- [36] AJMAL, A. et al. Principles and mechanisms of photocatalytic dye degradation on TiO₂ based photocatalysts: a comparative overview. **RSC Adv.**, v. 4, n. 70, p. 37003–37026, 2014.
- [37] GAYA, U. I.; ABDULLAH, A. H. Heterogeneous photocatalytic degradation of organic contaminants over titanium dioxide: A review of fundamentals, progress and problems. **Journal of Photochemistry and Photobiology C: Photochemistry Reviews**, v. 9, n. 1, p. 1–12, mar. 2008.
- [38] MA, Y. et al. Titanium Dioxide-Based Nanomaterials for Photocatalytic Fuel Generations. **Chemical Reviews**, v. 114, n. 19, p. 9987–10043, 8 out. 2014.
- [39] KHAN, H.; SHAH, M. U. H. Modification strategies of TiO2 based photocatalysts for enhanced visible light activity and energy storage ability: A review. **Journal of Environmental Chemical Engineering**, v. 11, n. 6, p. 111532, dez. 2023.
- [40] ŽERJAV, G. et al. Brookite vs. rutile vs. anatase: What's behind their various photocatalytic activities? **Journal of Environmental Chemical Engineering**, v. 10, n. 3, p. 107722, jun. 2022.
- [41] ZHANG, J. et al. New understanding of the difference of photocatalytic activity among anatase, rutile and brookite TiO₂. **Physical Chemistry Chemical Physics**, v. 16, n. 38, p. 20382–20386, 2014.
- [42] PARK, H. et al. Surface modification of TiO2 photocatalyst for environmental applications. **Journal of Photochemistry and Photobiology C: Photochemistry Reviews**, v. 15, p. 1–20, jun. 2013.
- [43] SEN, P. et al. Advancements in Doping Strategies for Enhanced Photocatalysts and Adsorbents in Environmental Remediation. **Technologies**, v. 11, n. 5, p. 144, 17 out. 2023.
- [44] PATTANAIK, P.; SAHOO, M. K. TiO2 photocatalysis: progress from fundamentals to modification technology. **Desalination and Water Treatment**, v. 52, n. 34–36, p. 6567–6590, out. 2014.
- [45] BALAPURE, A.; RAY DUTTA, J.; GANESAN, R. Recent advances in semiconductor heterojunctions: a detailed review of the fundamentals of photocatalysis, charge transfer mechanism and materials. **RSC Applied Interfaces**, v. 1, n. 1, p. 43–69, 2024.
- [46] ZHAO, Y. et al. Classification and catalytic mechanisms of heterojunction photocatalysts and the application of titanium dioxide (TiO2)-based heterojunctions in environmental remediation. **Journal of Environmental Chemical Engineering**, v. 10, n. 3, p. 108077, jun. 2022.
- [47] SAMY, M. et al. Understanding the variations in degradation pathways and generated by-products of antibiotics in modified TiO2 and ZnO photodegradation systems: A comprehensive review. **Journal of Environmental Management**, v. 370, p. 122402, nov. 2024.

- [48] ZHANG, G.; KIM, G.; CHOI, W. Visible light driven photocatalysis mediated via ligand-to-metal charge transfer (LMCT): an alternative approach to solar activation of titania. **Energy & Environmental Science**, v. 7, n. 3, p. 954, 2014.
- [49] KIM, G.; CHOI, W. Charge-transfer surface complex of EDTA-TiO2 and its effect on photocatalysis under visible light. **Applied Catalysis B:** Environmental, v. 100, n. 1–2, p. 77–83, 11 out. 2010.
- [50] FU, X. et al. Critical review on modified floating photocatalysts for emerging contaminants removal from landscape water: problems, methods and mechanism. **Chemosphere**, v. 341, p. 140043, nov. 2023.
- [51] DAI, L. et al. Floatable photocatalysts: Design principles and application advances. **Journal of Environmental Chemical Engineering**, v. 12, n. 4, p. 113029, ago. 2024.
- [52] ULLAH, S. et al. Supported nanostructured photocatalysts: the role of support-photocatalyst interactions. **Photochemical & Photobiological Sciences**, v. 22, n. 1, p. 219–240, 30 set. 2022.
- [53] SEIFIKAR, F.; HABIBI-YANGJEH, A. Floating photocatalysts as promising materials for environmental detoxification and energy production: A review. **Chemosphere**, v. 355, p. 141686, maio 2024.
- [54] SBOUI, M. et al. TiO 2 –PANI/Cork composite: A new floating photocatalyst for the treatment of organic pollutants under sunlight irradiation. **Journal of Environmental Sciences**, v. 60, p. 3–13, out. 2017.
- [55] HOSSEINI, S. N. et al. Immobilization of TiO2 on perlite granules for photocatalytic degradation of phenol. **Applied Catalysis B: Environmental**, v. 74, n. 1–2, p. 53–62, jun. 2007.
- [56] ALI, H. M.; ARABPOUR ROGHABADI, F.; AHMADI, V. Solid-supported photocatalysts for wastewater treatment: Supports contribution in the photocatalysis process. **Solar Energy**, v. 255, p. 99–125, maio 2023.
- [57] NAM, Y. S.; PARK, T. G. Porous biodegradable polymeric scaffolds prepared by thermally induced phase separation. **Journal of Biomedical Materials Research**, v. 47, n. 1, p. 8–17, out. 1999.
- [58] ÖNDER, Ö. C.; YILGÖR, E.; YILGÖR, I. Fabrication of rigid poly(lactic acid) foams via thermally induced phase separation. **Polymer**, v. 107, p. 240–248, dez. 2016.
- [59] BHATTACHARYYA, S. et al. Remediation of groundwater pollution using photocatalytic membrane reactors. **Groundwater for Sustainable Development**, v. 24, p. 101055, fev. 2024.
- [60] BIANCO, A. et al. Control of the Porous Structure of Polystyrene Particles Obtained by Nonsolvent Induced Phase Separation. **Langmuir**, v. 33, n. 46, p. 13303–13314, 21 nov. 2017.

- [61] PADILHA, L. F.; BORGES, C. P. PVC MEMBRANES PREPARED VIA NON-SOLVENT INDUCED PHASE SEPARATION PROCESS. **Brazilian Journal of Chemical Engineering**, v. 36, n. 1, p. 497–509, mar. 2019.
- [62] LI, L. et al. Novel Floating TiO₂ Photocatalysts for Polluted Water Decontamination Based on Polyurethane Composite Foam. **Separation Science and Technology**, v. 50, n. 2, p. 164–173, 22 jan. 2015.
- [63] HAN, H.; BAI, R. Buoyant Photocatalyst with Greatly Enhanced Visible-Light Activity Prepared through a Low Temperature Hydrothermal Method. **Industrial & Engineering Chemistry Research**, v. 48, n. 6, p. 2891–2898, 18 mar. 2009.
- [64] MAGALHÃES, F.; MOURA, F. C. C.; LAGO, R. M. TiO2/LDPE composites: A new floating photocatalyst for solar degradation of organic contaminants. **Desalination**, v. 276, n. 1–3, p. 266–271, ago. 2011.
- [65] ZHU, Z. et al. Fabrication of conductive and high-dispersed Ppy@Ag/g-C3N4 composite photocatalysts for removing various pollutants in water. **Applied Surface Science**, v. 387, p. 366–374, nov. 2016.
- [66] GUO, Y. et al. Developing polyetherimide/graphitic carbon nitride floating photocatalyst with good photodegradation performance of methyl orange under light irradiation. **Chemosphere**, v. 179, p. 84–91, jul. 2017.
- [67] ZHANG, L. et al. Multifunctional Floating Titania-Coated Macro/Mesoporous Photocatalyst for Efficient Contaminant Removal. ChemPlusChem, v. 80, n. 3, p. 623–629, mar. 2015.
- [68] SINGH, S.; SINGH, P. K.; MAHALINGAM, H. Novel Floating Ag⁺ Doped TiO₂ /Polystyrene Photocatalysts for the Treatment of Dye Wastewater. **Industrial & Engineering Chemistry Research**, v. 53, n. 42, p. 16332–16340, 22 out. 2014.
- [69] ATA, R. et al. Visible light active N-doped TiO2 immobilized on polystyrene as efficient system for wastewater treatment. **Journal of Photochemistry and Photobiology A: Chemistry**, v. 348, p. 255–262, nov. 2017.
- [70] ALTIN, İ.; SÖKMEN, M. Preparation of TiO2-polystyrene photocatalyst from waste material and its usability for removal of various pollutants. **Applied Catalysis B: Environmental**, v. 144, p. 694–701, jan. 2014.
- [71] SILVESTRI, S. et al. Synthesis of PPy-ZnO composite used as photocatalyst for the degradation of diclofenac under simulated solar irradiation. **Journal of Photochemistry and Photobiology A: Chemistry**, v. 375, p. 261–269, abr. 2019.
- [72] VAIANO, V.; MATARANGOLO, M.; SACCO, O. UV-LEDs floating-bed photoreactor for the removal of caffeine and paracetamol using ZnO supported on polystyrene pellets. **Chemical Engineering Journal**, v. 350, p. 703–713, out. 2018.

- [73] ACUÑA-BEDOYA, J. D. et al. Boosting visible-light photocatalytic degradation of polystyrene nanoplastics with immobilized CuxO obtained by anodization. **Journal of Environmental Chemical Engineering**, v. 9, n. 5, p. 106208, out. 2021.
- [74] GARCÍA-MUÑOZ, P. et al. Photocatalytic degradation of polystyrene nanoplastics in water. A methodological study. **Journal of Environmental Chemical Engineering**, v. 10, n. 4, p. 108195, ago. 2022.
- [75] SHANG, J.; CHAI, M.; ZHU, Y. Photocatalytic Degradation of Polystyrene Plastic under Fluorescent Light. **Environmental Science & Technology**, v. 37, n. 19, p. 4494–4499, 1 out. 2003.
- [76] VALDIVIESO-RAMÍREZ, C. S. et al. One-Step Synthesis of Iron and Titanium-Based Compounds Using Black Mineral Sands and Oxalic Acid under Subcritical Water Conditions. **Minerals**, v. 12, n. 3, p. 306, 28 fev. 2022.
- [77] MANCIC, L. T. et al. Precursor Particle Size as the Key Parameter for Isothermal Tuning of Morphology from Nanofibers to Nanotubes in the Na_{2-x} H_x Ti_n O_{2 n+1} System through Hydrothermal Alkali Treatment of Rutile Mineral Sand. Crystal Growth & Design, v. 9, n. 5, p. 2152–2158, 6 maio 2009.
- [78] GIL-LONDOÑO, J. et al. Extrinsic Point Defects in TiO₂ –Acetylacetone Charge-Transfer Complex and Their Effects on Optical and Photochemical Properties. **Inorganic Chemistry**, v. 62, n. 5, p. 2273–2288, 6 fev. 2023.
- [79] SCOLAN, E.; SANCHEZ, C. Synthesis and Characterization of Surface-Protected Nanocrystalline Titania Particles. **Chemistry of Materials**, v. 10, n. 10, p. 3217–3223, 1 out. 1998.
- [80] EL-SAMAK, A. A. et al. A stable porous vessel for photocatalytic degradation of Azocarmine G dye. **Microporous and Mesoporous Materials**, v. 341, p. 111994, ago. 2022.
- [81] SHAVISI, Y. et al. Application of TiO2/perlite photocatalysis for degradation of ammonia in wastewater. **Journal of Industrial and Engineering Chemistry**, v. 20, n. 1, p. 278–283, jan. 2014.
- [82] XING, Z. et al. A Floating Porous Crystalline TiO₂ Ceramic with Enhanced Photocatalytic Performance for Wastewater Decontamination. **European Journal of Inorganic Chemistry**, v. 2013, n. 13, p. 2411–2417, maio 2013.
- [83] FOSTIER, A. H. et al. Arsenic removal from water employing heterogeneous photocatalysis with TiO2 immobilized in PET bottles. **Chemosphere**, v. 72, n. 2, p. 319–324, maio 2008.
- [84] ROSA, D. et al. Iron-doped titania nanoparticles supported on polystyrene for photocatalytic treatment of contaminated water in a continuous system. **Journal of Photochemistry and Photobiology A: Chemistry**, v. 447, p. 115241, jan. 2024.

- [85] MANJUNATHA, M.; MAHALINGAM, H. Upcycling of waste EPS beads to immobilized codoped TiO2 photocatalysts for ciprofloxacin degradation and E. coli disinfection under sunlight. **Scientific Reports**, v. 13, n. 1, p. 14631, 5 set. 2023.
- [86] HABRAN, M. et al. Visible light sensitive mesoporous nanohybrids of lepidocrocite-like ferritianate coupled to a charge transfer complex: Synthesis, characterization and photocatalytic degradation of NO. **Journal of Photochemistry and Photobiology A: Chemistry**, v. 365, p. 133–144, out. 2018.
- [87] HIDAKA, H.; ZHAO, J. Photodegradation of surfactants catalyzed by a TiO2 semiconductor. **Colloids and Surfaces**, v. 67, p. 165–182, nov. 1992.
- [88] ABEBE, B.; MURTHY, H. C. A.; AMARE, E. Summary on Adsorption and Photocatalysis for Pollutant Remediation: Mini Review. **Journal of Encapsulation and Adsorption Sciences**, v. 08, n. 04, p. 225–255, 2018.
- [89] AMBROZ, F. et al. Evaluation of the BET Theory for the Characterization of Meso and Microporous MOFs. **Small Methods**, v. 2, n. 11, p. 1800173, nov. 2018.
- [90] SUN, Z.-X. et al. Effects of calcination temperature on the pore size and wall crystalline structure of mesoporous alumina. **Journal of Colloid and Interface Science**, v. 319, n. 1, p. 247–251, mar. 2008.
- [91] YIASE, S. G.; ADEJO, S. O.; ININGEV, S. T. Manganese (II) and Cobalt (II) Acetylacetonates as Antimicrobial Agents. **NIGERIAN ANNALS OF PURE AND APPLIED SCIENCES**, v. 1, p. 176–185, 14 mar. 2019.
- [92] SIWIŃSKA-STEFAŃSKA, K. et al. The influence of addition of a catalyst and chelating agent on the properties of titanium dioxide synthesized via the sol–gel method. **Journal of Sol-Gel Science and Technology**, v. 75, n. 2, p. 264–278, ago. 2015.
- [93] YANG, G.; LANG, Y. Photodegradation of Antibiotic Drugs by BiVO4 Nanocomposites. **Materials Science**, v. 29, n. 4, p. 507–514, 1 dez. 2023.
- [94] ZHU, X.-D. et al. Photocatalytic degradation of tetracycline in aqueous solution by nanosized TiO2. **Chemosphere**, v. 92, n. 8, p. 925–932, ago. 2013.
- [95] PATIDAR, A. et al. Reactive oxygen species aided photocatalytic degradation of tetracycline using non-metal activated carbon doped TiO2 nanocomposite under UV-light irradiation. **Research on Chemical Intermediates**, v. 50, n. 3, p. 1035–1063, mar. 2024.
- [96] WU, S. et al. Visible light photocatalytic degradation of tetracycline over TiO2. **Chemical Engineering Journal**, v. 382, p. 122842, fev. 2020.
- [97] SHI, F. et al. Formation of core/shell structured polystyrene/anatase TiO2 photocatalyst via vapor phase hydrolysis. **Applied Catalysis B: Environmental**, v. 123–124, p. 127–133, jul. 2012.

[98] QIN, X. et al. Enhanced photocatalytic activity for degrading Rhodamine B solution of commercial Degussa P25 TiO2 and its mechanisms. **Journal of Hazardous Materials**, v. 172, n. 2–3, p. 1168–1174, dez. 2009.